61p

[redacted]

OTS PRICE

XEROX $ 6.60 ph.

MICROFILM $ _____

EXOTECH
INCORPORATED

4208 WHEELER AVENUE • ALEXANDRIA, VIRGINIA

SGT M. Tubin

INVESTIGATION OF A MICROMETEOROID VEHICLE DAMAGE ASSESSMENT SYSTEM

BY:

W. C. Cooley
P. G. Luckhardt
R. J. Janda
P. E. Brockert

Summary Report

on Contract NAS 8-5033
for the National Aeronautics and Space Administration
Marshall Space Flight Center
Huntsville, Alabama

Exotech Incorporated
4208 Wheeler Avenue
Alexandria, Virginia

June 1963

TECHNICAL REPORT
TR-004

TABLE OF CONTENTS

LIST OF FIGURES

LIST OF TABLES

2358

ABSTRACT

A laboratory calibration model of a meteoroid puncture detection system has been developed which can be used to measure the visible and infrared radiation produced by "puncture flash" in hypervelocity impact facilities. Research is reported on the infrared and visible radiation signals obtained from punctures of steel, Pyrex and sapphire spheres through 50 mil aluminum in vacuum, air, helium, gaseous oxygen and liquid oxygen. The nature of puncture flash phenomena is discussed, and conclusions are drawn as a result of correlation of the test data. Author

II. INTRODUCTION

Since May 1962, research has been conducted under Contract NAS 8-5033 to investigate the use of infrared and visible sensors to detect the "puncture flash" of radiation emitted inside a tank when it is punctured by a hypervelocity particle, simulating a meteoroid. The results of the first phase of this program (Ref. 1) showed that a meteoroid puncture detection system using lead sulfide photoconductive infrared sensors was feasible. Additional efforts in the period from November 1962 to June 1963, which are reported herein, have resulted in the development of a portable laboratory calibration model of a puncture detection system and have accumulated additional research data on the nature of puncture flash phenomena in vacuum, in various gases, and in liquid oxygen.

Concurrently, research conducted under Contract NAS 9-1268 entitled, "Investigation Of Feasibility Of Detecting Meteoroid Punctures In Atlas Tanks" has provided additional data on puncture flash phenomena (Ref. 2) which supplement the results reported here and therefore have aided in drawing conclusions concerning the nature of the phenomena.

As used in this report, the term "puncture flash" refers to the radiation emitted on the rear (exit) side of a target which is punctured, as distinguished from the term "impact flash" which has been used in the literature primarily to denote radiation emitted on the front (entrance) side of the target by either a penetrating or a non-penetrating impact.

The following topics are covered in this report:

A. Physics of Impact Flash and Puncture Flash Phenomena

B. Experimental Program

C. Development of a Laboratory Calibration Model of a Meteoroid Puncture Detection System

III. PHYSICS OF IMPACT FLASH & PUNCTURE FLASH PHENOMENA

A. Review of Impact Flash Literature

When a particle at a velocity of approximately 5000 ft/sec or greater impacts a solid surface, a flash of visible radiation is observed from the impact point. Atkins (Ref. 3) photographically recorded the impact flash on the front (entrance) side of a 1/2 inch aluminum target plate when punctured by a 1/2 inch steel sphere at 5000 ft/sec. The luminous flash emanates from an annular region around the impact point and is accompanied by ejection of small spray particles from the front side of the target primarily at a cone angle of approximately 60° to 70° from the trajectory. These solid spray particles may have a velocity two to three times greater than the impact velocity.

Spectral analyses of the impact flash have been conducted at the University of Utah (Ref. 4), the General Motors Defense Research Laboratories (Ref. 5 and 6), McGill University (Ref. 7), and at the NASA Ames Research Center (Ref. 8). The spectra obtained from impact of metal and nylon projectiles on metallic and solid rock targets show spectral lines associated with the elements composing the target. However, when nylon impacted a sand target at $\sim$ 10,000 ft/sec (Ref. 6) no line spectra were observed, but only a continuum in the near infrared.

Gehring and Charters (Ref. 6) observed impact flash with visible and infrared photomultiplier tubes and found that the peak luminosity was proportional to the square of the projectile diameter and to the impact velocity raised to a power from 3 to 9, depending on the projectile and target material. They found the luminosity of impact flash in air at 10 Torr pressure to be independent of projectile mass and material, with the exception of Pyrex spheres on aluminum which gave a factor of three lower luminosity than for solid or hollow metallic spheres of the same outside diameter.

Research with photomultipliers and spectrographs has been conducted to determine whether there is an effect of the gas atmosphere on the impact flash. This question is relevant to the detection of the impact of vehicles or meteoroids on the moon, and also is pertinent to the detection of meteoroid impacts on, or punctures through, the skin of space vehicles.

Experiments by Clark, Kadisch and Grow (Ref. 4) showed a line spectrum which was attributed to reaction of the surrounding gas with the high-velocity spray thrown out of the crater during the crater's formation. For impacts of copper spheres into copper targets at 2.2 km/sec, they observed atomic copper lines at 60 Torr pressure of Argon, but no lines and two orders of magnitude lower intensity at 635 Torr pressure of hydrogen. They concluded that impact flash results primarily from the collisions between spray particles and the surrounding atmosphere. However, Gehring and Charters (Ref. 6) report no significant effect of the pressure of a helium gas environment on the magnitude of the impact flash for nylon projecticles on sand targets in the velocity range from 2.1 to 3.1 km/sec at pressures of 10^{-3} to 200 Torr. Their data show no effect of pressure or gas composition for impacts of aluminum on aluminum in both helium and in air at pressures below 0.1 Torr. However, their data for Al on Al at 8000 ft/sec show an increase in luminosity with air pressure which becomes significant at pressures of 10 Torr and higher, indicating that reaction with air adds to the visible radiation.

MacCormack (Ref. 8) has studied the initial rate of rise of the visible impact flash radiation from impacts of aluminum spheres on both aluminum and basalt rock targets. He reported that in the air pressure range from 4×10^{-4} to 0.2 Torr, the initial rate of increase of luminosity increased approximately as the cube root of the ambient pressure. However, inspection of his data shows that it is not inconsistent with an assumption that the luminosity could become independent of pressure at a pressure of the order of 10^{-3} Torr.

MacCormack has calculated the velocity of an aluminum atom required to produce the first excited state of an outer aluminum electron upon collision with another atom, which would lead to the observable aluminum spectral line at 3962 Angstroms. He calculates velocities of 6.6 km/sec in Nitrogen, 6.1 km/sec in Argon, 13.2 km/sec in helium, 17.9 km/sec in hydrogen, and 6.7 km/sec in aluminum vapor. He experimentally observed the aluminum line at an impact velocity of 2.5 km/sec in air at 8×10^{-4} Torr, which implies a fairly large number of aluminum atom collisions at velocities greater than 6.6 km/sec, which is 2.6 times the impact velocity. He observes that solid spray particles have been observed to travel as much as three times

the impact speed, which may be expected to radiate in the same manner as meteors if a gas is present. In addition, one should consider that the atoms of aluminum vapor released on impact will have a velocity distribution (although perhaps not Maxwellian) so that some atomic collisions can be expected at relative velocities even greater than three times the impact velocity. Therefore, solid ejecta particles reacting with a gas atmosphere and atoms of the target and pellet vapor interacting with each other and with the gas atmosphere probably contribute to line spectra. Since the density of the shock-produced vapor is much higher than that of the surrounding gas during the early stages of impact flash, one would expect line spectra to be dominated by interatomic collisions between vapor atoms, rather than collisions of vapor atoms with the surrounding gas. However, at a sufficiently high gas pressure, one would expect the collisions between vapor atoms and gas atoms to become dominant, at least during the later stages of the impact flash when the vapor cloud has expanded nearly to the ambient pressure.

MacCormack suggests that in the experiments of Gehring and Sieck (Ref. 5) with nylon projecticles into sand, the luminosity produced by ejecta interacting with the atmosphere may not constitute a significant amount of radiation as compared to the "radiation produced by the mechanics of cratering." This argument is consistent with MacCormack's results which show a pressure dependence for Al on Al beginning at lower pressures ($\sim 10^{-3}$ Torr). than Gehring and Charters found for Nylon on Al ($\sim$0.1 to 10 Torr). However, if a basic component of the radiation which is "produced entirely by the mechanics of cratering" actually exists, as assumed by MacCormack in discussing Gehring's data, one would predict that MacCormack's data should show independence of pressure below some value, possibly near 10^{-3} Torr. It is believed that further measurements of the pressure dependence of impact flash would be desirable in order to understand the effect of a gas environment on impact flash.

B. Theory of Impact Phenomena

Theoretical studies of the hypervelocity impact of pellets which puncture thin plates, like meteoroid bumpers, has been conducted by Bull (Ref. 9) and by Friend, Millar, and Murphy (Ref. 10) at McGill University. The detailed description of the penetration process is extremely complicated, but may be described qualitatively as follows:

When a pellet strikes a thin target at high velocity, a shock wave is generated which passes into the target and back through the pellet. The pressure and temperature generated by the shock wave can be approximated by applying the laws of conservation of energy and momentum and the equations of state of the materials (if known).

For a one dimensional shock wave at sufficiently high velocities that the latent heat of vaporization may be neglected, the shocked material may be treated as a polytropic gas, leading to the Rankine-Hugoniot pressure - density relations. Assuming very strong shock waves, relations can be derived (Ref. 9) expressing the material velocity behind the shock, the shock wave velocities and the pressure behind the shock, which is found to be proportional to the square of the pellet impact velocity. The temperature generated by the shock can also be calculated and is also found to vary as the square of the pellet impact velocity. It is expected that these ideal approximations may be reasonably valid at impact velocities greater than 10 km/sec, which are applicable for meteoroids which have velocities from 11 to 72 km/sec. However, they are probably not very accurate at lower velocities of 2 to 8 km/sec which are attainable in the laboratory. At these lower velocities the simple theory predicts temperatures which may be an order of magnitude too high (Ref. 9, p. 18).

The simple theory yields an impact pressure for identical pellet and target material given by

$$P = \frac{1}{2} \rho_0 V^2$$

where ρ_0 is the density of the pellet and target material and V is the pellet impact velocity. This yields a pressure of 4 megabars for an iron pellet impacting iron at 10 km/sec, which checks closely with Bjork's result (Ref. 11), assuming a ratio of specific heats of $\gamma = 3$ for the condensed medium.

The corresponding temperature is estimated from the equation:

$$T = \frac{(\gamma - 1) V^2}{8R}$$

where R is the gas constant for the condensed medium.

The equation yields a temperature of about 168,000°K for iron on iron at 10 km/sec and 80,000°K for Al on Al at 10 km/sec. If the equation still applies at a velocity of 2.5 km/sec, the temperatures are 10,500°K for Fe on Fe and 5000°K for Al on Al. However, these temperatures are probably too high because proper account is not taken of the heats of fusion and vaporization which tend to lower the temperature.

The theory cannot be expected to be accurate because it does not take into account departures from thermodynamic equilibrium, and electron stripping and Bremstrahlung production which probably exist at the higher impact velocities. Bull (Ref. 7) has observed visible spectra and 3 cm wave radiation generated by impacts of Mg on Mg, Cu on Cu, Al on Al and Brass on Brass at velocities near 30,000 ft/sec (9km/sec). He finds that the visible line spectra are not unreasonable in terms of the estimated temperatures, but that there appears to be considerable long wavelength emission, possibly from ion-oscillations in the impact generated plasma. He observes that the total intensity of visible light generated behind a thin target is of similar intensity to that observed from the front side.

C. Description of Puncture Flash

The intensity, spectral distribution and time variation of radiation emitted behind a thin target by a high velocity puncture is determined by the complex behavior of the ejected material, which includes solid particles, vaporized material and possibly liquid. The measured radiation parameters are a function of the view angle and field of view of the sensor as well as the pellet and wall properties and the pressure and composition of the gas or liquid into which the puncture occurs. Unless care is taken in experimental work to reduce the view angle or to use very rapid response sensors, the impact flash produced by solid ejecta on the inside of the target tank will be confused with that produced by the ejecta material directly, since the former usually predominates.

Typically the ejecta emit visible light from a conical region behind the target. Upon impact of solid ejecta particles with a secondary target (a back-spatter plate or witness plate), a roughly hemispherical region of plasma is produced which may have a total luminosity exceeding that of the ejecta cone. In addition, streaks of light may be observed emanating from the back-spatter plate which are analogous to those observed from spray particles on the front side of a plate after a primary impact.

The radiant intensity and effective color temperature of the ejecta cone and of the impact flash produced by solid ejecta is extremely variable, but generally the average intensity and color temperature decrease as the kinetic energy of impact is reduced. For barely penetrating impacts at 7500 ft/sec into vacuum, no visible radiation is observed behind the target, although a lead sulfide photoconductive sensor can detect the infrared radiation at a range of 36 feet (Ref. 2). It is found that the visible and infrared radiation

observed behind a target generally increases as the target thickness is reduced, indicating that a larger fraction of the shock produced plasma is ejected through the target, and that the higher kinetic energy of ejecta particles leads to more intense radiation when they impact the back spatter plate.

A more complete description of the test results obtained when firing into various media is given in the following section.

IV. EXPERIMENTAL PROGRAM

A. Experiments With 220 Swift Powder Gun in Vacuum and in Various Tank Environments

Modifications were made to the 220 Swift powder gun facility described in Reference 1 to permit measurements at pressures down to 4×10^{-4} Torr by using a stainless target chamber, pumped by a Welsh Turbomolecular vacuum pump. The tank design is shown in Figure 1 and 2 and a photograph is shown in Figure 3. Vacuum measurements were made with a McLeod guage.

Spheres of stainless steel, sapphire and Pyrex were fired through 0.050 inch thick aluminum diaphragms at a velocity of 7500 ft/sec ($\pm$ 5%). Also, one shot of a 1/32 inch sapphire sphere was made through a 0.020 inch thick Type 301 full-hardened stainless steel sheet for comparison with a similar shot made at the Naval Research Laboratory at a higher velocity of 17,000 ft/sec.

Gun velocity was measured by oscilloscope timing from the appearance of visible radiation at the gun muzzle as detected by a silicon photovoltaic sensor, to the appearance of the puncture flash at the target diaphragm at a distance of 90 inches.

Puncture flash measurements and oscillogram records were made of the visible radiation with an RCA Type 6199 photomultiplier tube, which responds in the wavelength range from 0.32 to 0.54 microns, and with Infrared Industries Sidewinder type lead sulfide photoconductive infrared sensors, which respond at all wavelengths up to approximately 2.5 microns.

In all cases an aluminum back spatter plate was located as shown in Figure 2 so that the sensors did not have a direct view of the impact point of ejecta particles. However, it is probable that in most cases, the plasma generated at the back spatter plate may have expanded into the field of view of the sensors. (See Sect. C-2 below)

The atmosphere inside the tank was varied to include vacuum below 10^{-3} Torr, standard atmosphere, helium gas, oxygen gas, and liquid oxygen.

A total of 128 shots were fired, resulting in 17 clean, sabot-free punctures for which 16 sets of valid test data were obtained. Typical oscillograms obtained from the firings are shown in Figures 4 through 7.

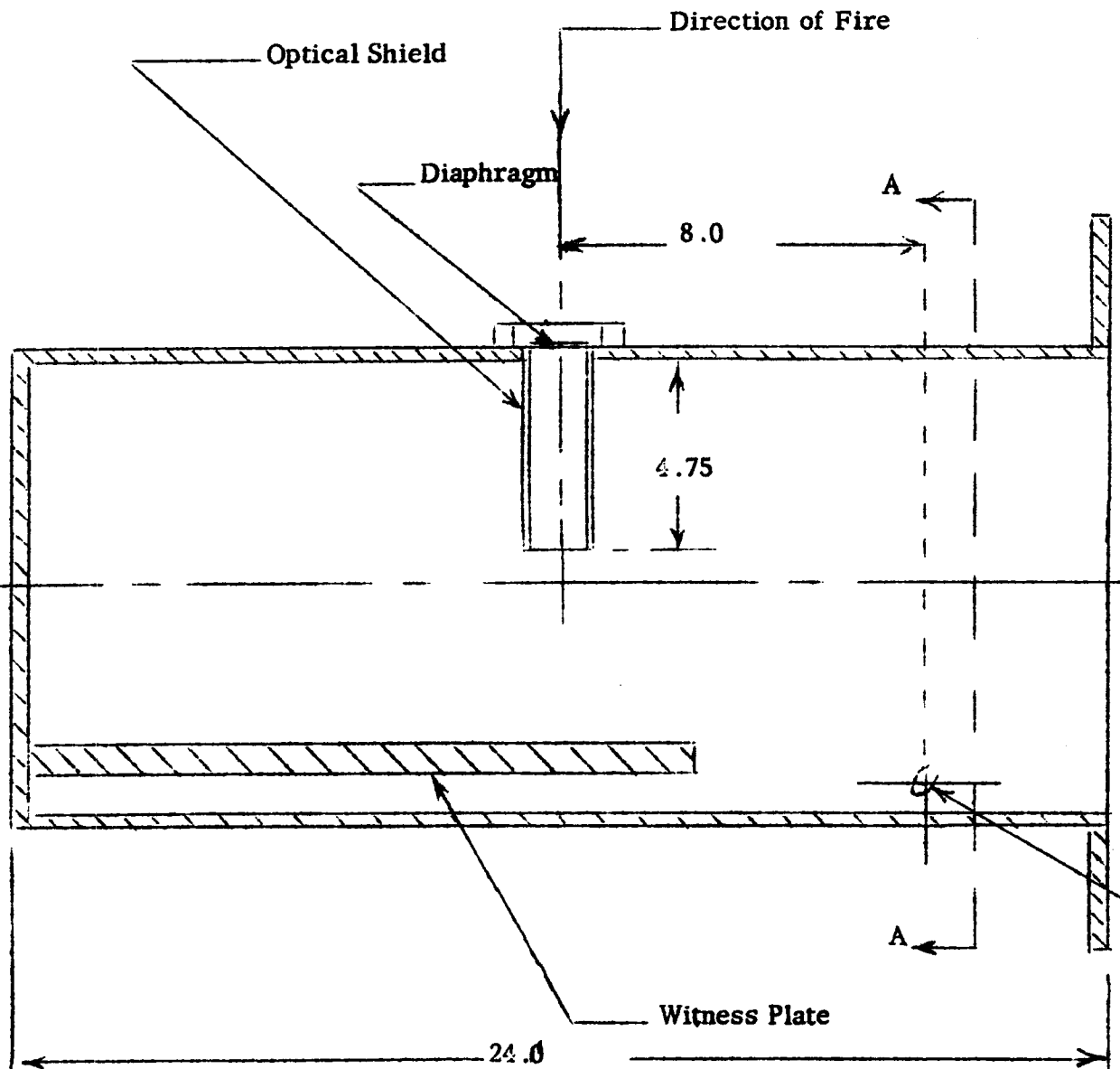

EXOTECH SIMULATOR RECEIVER TANK - CROSS SECTION

Figure 1

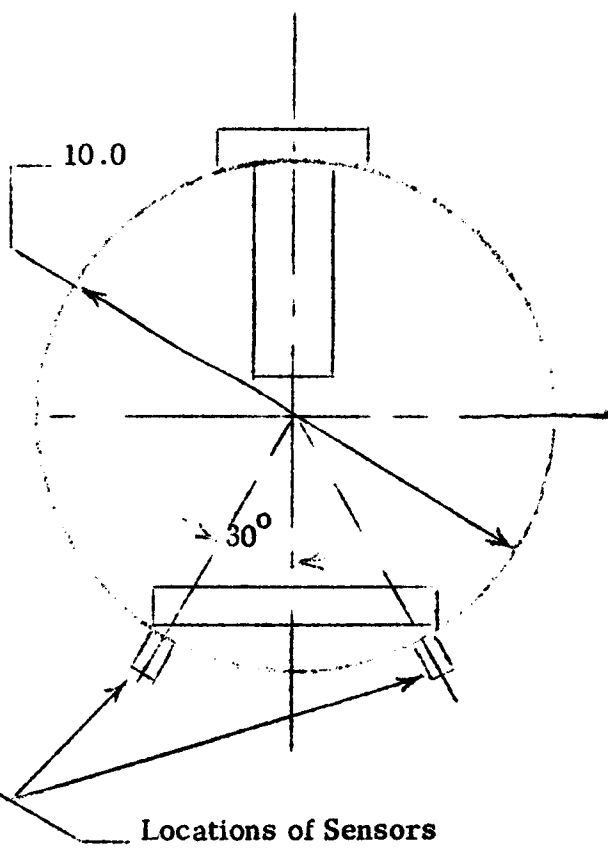

Section A - A

RECEIVER TANK END VIEW

Figure 2

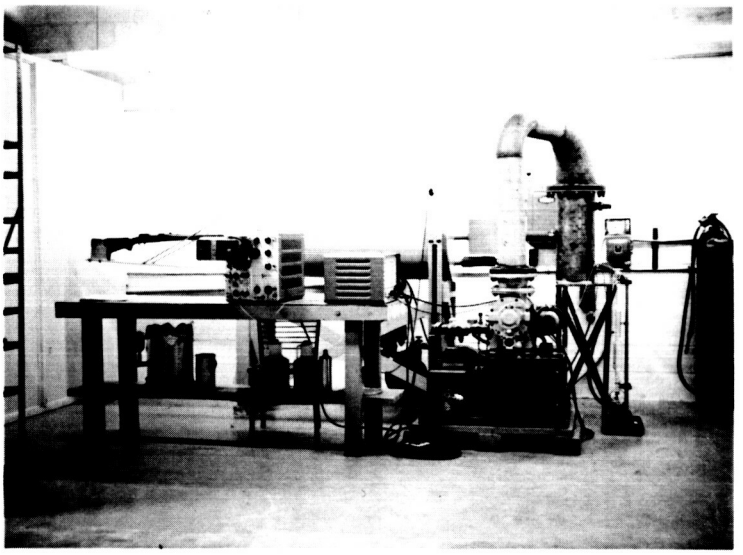

Figure 3

Photograph Of Exotech Simulator Facility

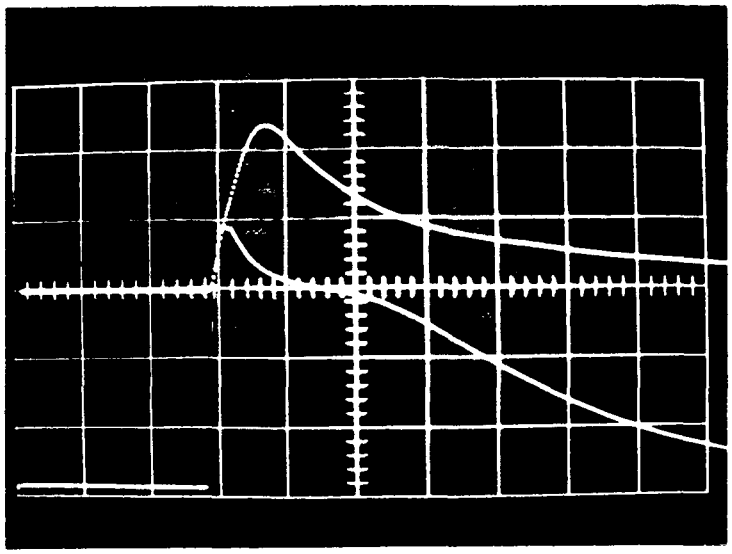

Figure 4

Oscillogram of Puncture Flash, Sidewinder Sensor and Photomultiplier (RCA-6199). .039" Steel ball through .050" Al. in Air (1 Atm.) No optical shield, 7500 ft/sec.
PbS - Upper Trace: Vertical Gain - 0.1v/cm.
PM - Lower Trace: Vertical Gain - 2v/cm.
Sweep - 0.5 ms/cm.

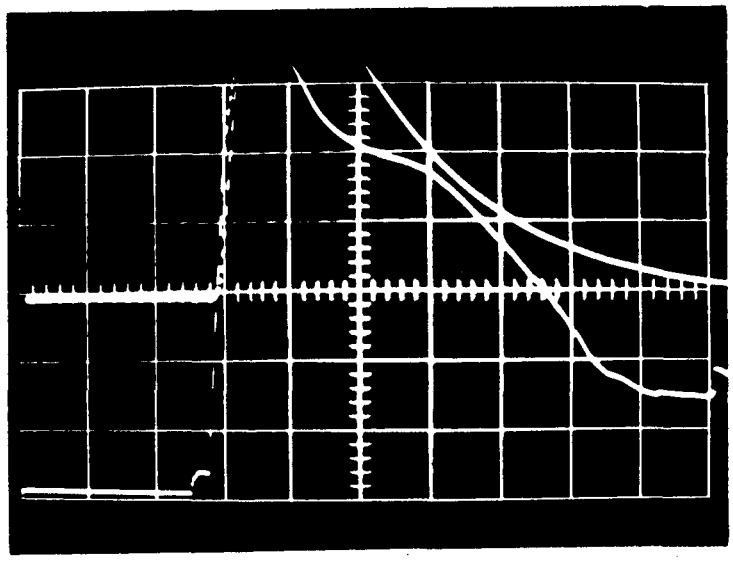

Figure 5

Oscillogram of Puncture Flash, Sidewinder Sensor and Photomultiplier (RCA-6199). .039" Steel ball through .050" Al. in Gaseous Oxygen (1 Atm.) No optical shield, 7500 ft/sec.
PbS - Upper Trace: Vertical Gain - 1v/cm.
PM - Lower Trace: Vertical Gain - 5v/cm.
Sweep - 0.5 ms/cm.

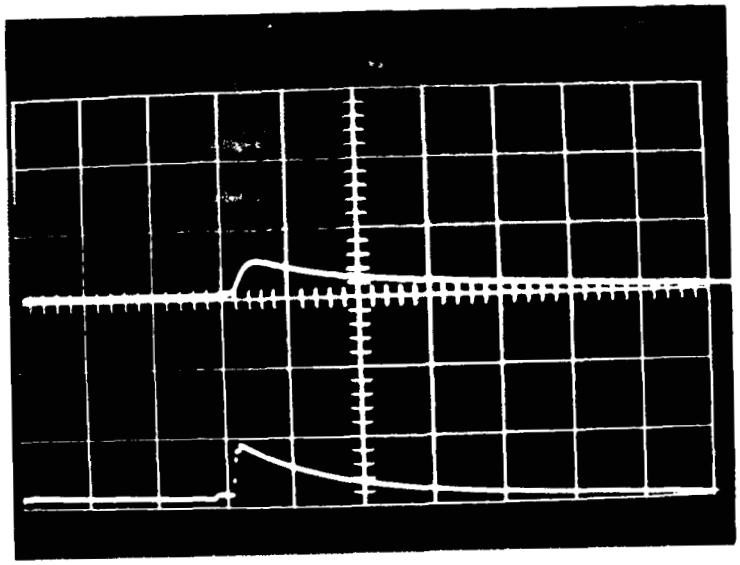

Figure 6

Oscillogram of Puncture Flash, Sidewinder Sensor and Photomultiplier (RCA-6199). .039" Steel ball through .050" Al. in Helium (1 Atm.) No optical shield, 7500 ft/sec.
PbS - Upper Trace: Vertical Gain - 0.1v/cm.
PM - Lower Trace: Vertical Gain - 2v/cm.
Sweep - 0.5 ms/cm.

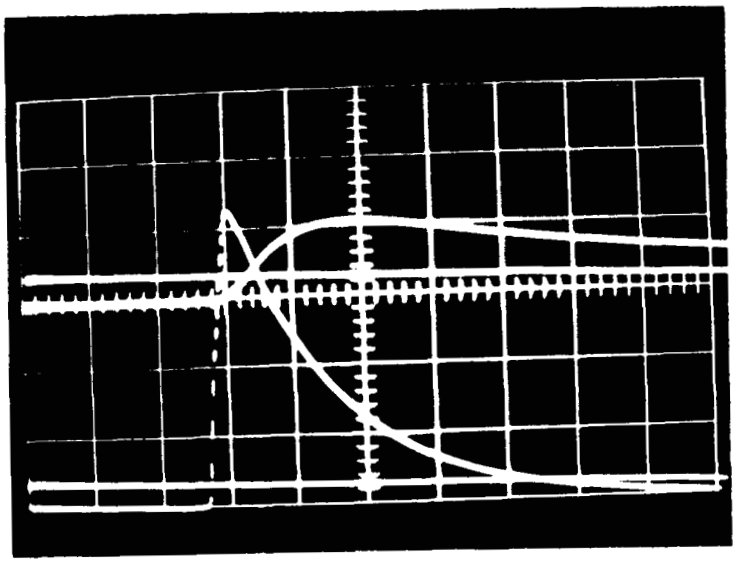

Figure 7

Oscillogram of Puncture Flash, Sidewinder Sensor and Photomultiplier (RCA-6199). 1/16" Sapphire ball through .050" Al. at 4×10^{-4} Torr, Optical shield (1-3/8" x 5" cylinder), 7500 ft/sec.
PbS - Upper Trace: Vertical Gain - 0.5v/cm.
PM - Lower Trace: Vertical Gain - 10v/cm.
Sweep - 0.5 ms/cm.

B. Experiments With The Naval Research Laboratory Hydrogen Gas Gun

With the cooperation of personnel of the Naval Research Laboratory, photomultiplier and infrared sensor measurements were made with Exotech instrumentation during 12 firings of 3/16 inch diameter steel and aluminum spheres through aluminum sheets, using the hydrogen gas gun at Range #5 of the NRL Mechanics Division. However, in each case, pieces of Lexan sabot punctured the target, invalidating the visible and infrared sensor measurements which were obtained. However, during experimentation conducted under Contract NAS 9-1268 (Ref. 2) a valid oscillogram was obtained in which both a photomultiplier and infrared signal were recorded for a 1/32 inch sapphire sphere at 17,000 ft/sec through 0.020 inch type 301 full-hardened stainless steel. The oscillogram is shown in Figure 8.

C. Experimental Results of Puncture Flash Measurements

1. Experimental Data

The experimental values of photomultiplier tube and infrared sensor signal amplitudes which were obtained during the test program are shown in Table I. The first seven shots were made with no optical shield so that both the PM tube and the IR sensor could view the rear face of the target diaphragm at a range of 12.4 inches and a view angle of 40° away from the normal to the sensitive face of the sensors.

The last nine shots were made with a 1-3/8" I.D. by 5 inch long tubular optical shield behind the target diaphragm, which prevented the sensor from seeing the ejecta until they had traveled to a point which was at a range of 9.5 inches and a view angle of 60° away from the normal to the sensors.

Since small variations in battery supply voltages occurred with time, the test data were normalized to standard supply voltages before comparison by assuming a constant responsivity (a linear variation of signal with supply voltage). The data as corrected to correspond to a constant photomultiplier applied voltage of 900 volts and a constant infrared sensor circuit voltage of 67.5 volts (of which one-half is applied to the sensor) are also tabulated in Table I.

2. The data on puncture flash for 0.025" and 0.039" steel spheres puncturing 0.050" aluminum at 7500 ft/sec are shown in Figure 9. It is seen that the PbS signal appears to vary as the seventh power of sphere diameter (the 2.3 power of mass or

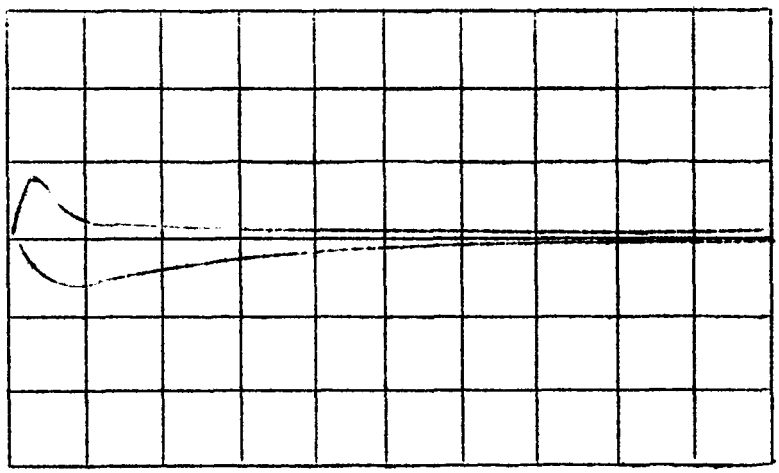

Figure 8

Oscillogram of Puncture Flash, Sidewinder Sensor and Photomultiplier Tube

1/32" sapphire ball through 0.0204" stainless steel (full hard, type 301): 3 Torr, 21.5" Range, 17,000 ft/sec (NRL)

Upper Trace: Photomultiplier Tube (RCA 6199)
Vertical Gain - 5V/cm

Lower Trace: Sidewinder Sensor (PbS). Vertical Gain: 0.5V/cm

Sweep: 0.5 ms/cm

TABLE I. Puncture Flash Test Data At 7500 feet/second

Shot Number	Tank Environment	Sphere	Target	Recorded Sensor Data: Channel 'A' Type, Bias, Scope Input	Channel 'A' Signal	Channel 'B' Type, Bias, Scope Input	Channel 'B' Signal	Signal Ratio	Corrected Data: PbS @ 67.5v V_{PbS}	PM @ 900v V_{PM}	Corrected Ratio $\frac{V_{PM}}{V_{PbS}}$
Group I - No Optical Shield											
5/14 B	Air-1 atm.	0.025" steel	0.050" Al*	-	-	PM 900v DC	2.6v	-	-	2.6v	-
5/15 I	LOX-above target, below sensors	0.025" steel	0.050" Al	-	-	PM 900v AC	>40v	-	-	>40v	-
5/16 C	LOX-below target Sensor A in gas Sensor C in LOX	0.025" steel	0.050 Al	PbS 88v AC	0.1v	PbS 90v AC	<0.01v	N/A	0.08v	<0.01v	N/A
5/17 D	Air-1 atm.	0.025" steel	0.050" Al	PbS 67.5v AC	0.01v	PM 900v AC	Off Scale	-	0.08v	Off Scale	-
5/17 F	Air-1 Atm.	0.039" steel	0.050" Al	PbS 67.5v AC	0.24v	PM 900v AC	7.6v	32	0.24v	7.6v	32
5/17 G	Helium-1 Atm.	0.039" steel	0.050" Al	PbS 67.5v AC	0.05v	PM 900v AC	1.6v	32	0.05v	1.6v	32
5/17 I	Oxygen-1 Atm.	0.039" steel	0.050" Al	PbS 67.5v AC	4v	-	-	-	4v	-	-

* Type 3003-H14

TABLE I - CONTINUED

Shot Number	Tank Environment	Sphere	Target	Recorded Sensor Data: Channel 'A' Type, Bias, Scope Input	Channel 'A' Signal	Channel 'B' Type, Bias, Scope Input	Channel 'B' Signal	Signal Ratio	Corrected Data: PbS @ 67.5v V_{PbS}	PM @ 900v V_{PM}	Corrected Ratio $\frac{V_{PM}}{V_{Pbs}}$
Group II - With 1-3/8" I.D. by 5" Long Optical Shield											
5/23 B	5 x 10^{-4} Torr (Air)	0.039" steel	0.050" Al*	PbS 90v AC	1.4v	PM 930v AC	20v	14	1.05v	19.3v	18.4
5/27 L	6 x 10^{-4} Torr (Air)	1/16" steel	0.050" Al	PbS 67.5 AC	3.6v	PM 830v AC	51v	14	3.6v	55v	15
5/29 I	4 x 10^{-4} Torr (Air)	1/16" sapphire	0.050" Al	PbS 70v AC	0.5v	PM 800v AC	43v	86	0.5v	48v	96
6/3 F	4 x 10^{-4} Torr (Air)	1/16" Pyrex	0.050" Al	PbS 70v AC	0.3v	PM 830v AC	0.4v	1.3	0.3v	0.43v	14
6/4 H	1 Torr (Air)	1/32" sapphire	0.020" 301 full-hard ss	PbS 70v AC	0.025v	PM 520v AC	1v	40	0.024v	1.7v	71
6/5 D	5 x 10^{-4} Torr (Air)	0.039" steel	0.050" Al	PbS 70v AC	4v	PM 540v AC	2.1v	5.25	0.4v	3.5v	9
6/5 H	3 Torr (Air)	1/32" sapphire	0.050" Al	PbS 70v AC	0.02v	PM 790v	>1.2	>60	0.02v	>1.3v	>65
6/6 F	Oxygen-1 Atm.	0.039" steel	0.050" Al	PbS 70v AC	2v	PM 710v AC	>60v	>30	1.9v	>76	>40
6/6 I	Oxygen-1 Atm.	0.039" steel	0.050" Al	PbS 70v AC	1.4v	PM 710v AC	62v	44	1.4v	78v	56

* Type 3003-H14

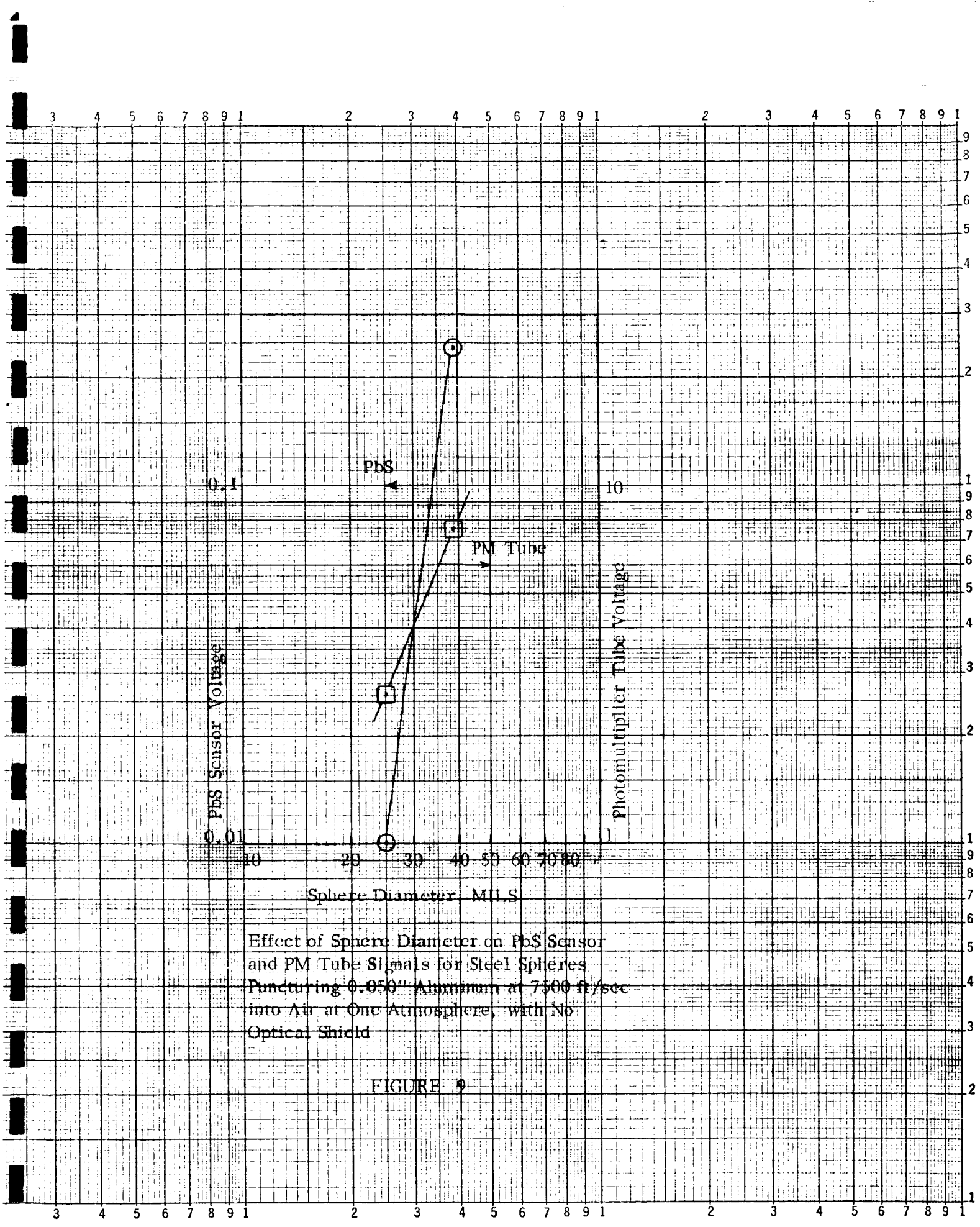

Effect of Sphere Diameter on PbS Sensor and PM Tube Signals for Steel Spheres Puncturing 0.050" Aluminum at 7500 ft/sec into Air at One Atmosphere, with No Optical Shield

FIGURE 9

kinetic energy) while the visible photomultiplier signal varies only as the 2.4 power of sphere diameter. However, it should be noted that the 0.025" steel sphere has only slightly greater kinetic energy than that required to puncture the plate and therefore, based on data from Reference 2, one does not expect a simple power law variation of PbS signal with mass or kinetic energy in this range.

The effect of various gas environments, helium, air and oxygen, on the puncture flash signals for punctures by 0.039 inch steel spheres through 0.050 inch aluminum are shown in Figure 10. It is seen that the data show a definite increase in amplitude for air and particularly for oxygen as compared to helium. The data have been plotted against oxygen partial pressure, which suggests that chemical oxidation reactions can contribute greatly to the total puncture flash radiation.

Figure 11 shows the time variation of the visible photomultiplier traces for punctures of 0.039 inch steel spheres through 0.050 inch aluminum into gaseous oxygen and helium. These oscillograph data which are copied from Figures 5 and 6 show very clearly that the ejecta cone itself, which is visible for the first 125 microseconds after impact, contributes a very small amount of light compared to the radiation flash produced by the secondary ejecta particles as they hit the back-spatter plate. It is also seen that the ejecta cone luminosity is enhanced by a factor of 7.5 and the peak luminosity by a factor of 22 in oxygen as compared to helium.

Surprisingly, the corresponding oscillogram (5/17F) as shown in Figure 4 for impact into air, shows no visible trace of ejecta cone radiation prior to the main radiation flash.

3. Firings into Liquid Oxygen

Figure 12 (shot 5/15I) shows the oscillogram taken when firing a 0.025" steel sphere through a 0.050" aluminum sheet into liquid oxygen which had its liquid level about one inch above the puncture point. The PM tube and PbS sensors therefore looked down through the liquid to the puncture point. It is seen that the photomultiplier tube signal went off scale, exceeding 50 volts and the PbS signal (which is downward in this case) shows about 0.2 volts from the ejecta cone and a 1 volt maximum amplitude which is sustained for at least 3 milliseconds. In this shot, the aluminum diaphragm

FIGURE 10

Effect of Helium, Air and Oxygen on Amplitude of Puncture Flash Signals on PbS Sensor and Visible Photomultiplier Tube

Data: 0.039" Steel Spheres Puncturing 0.050" AL Sheet at 7500 ft/sec.
No Optical Shield

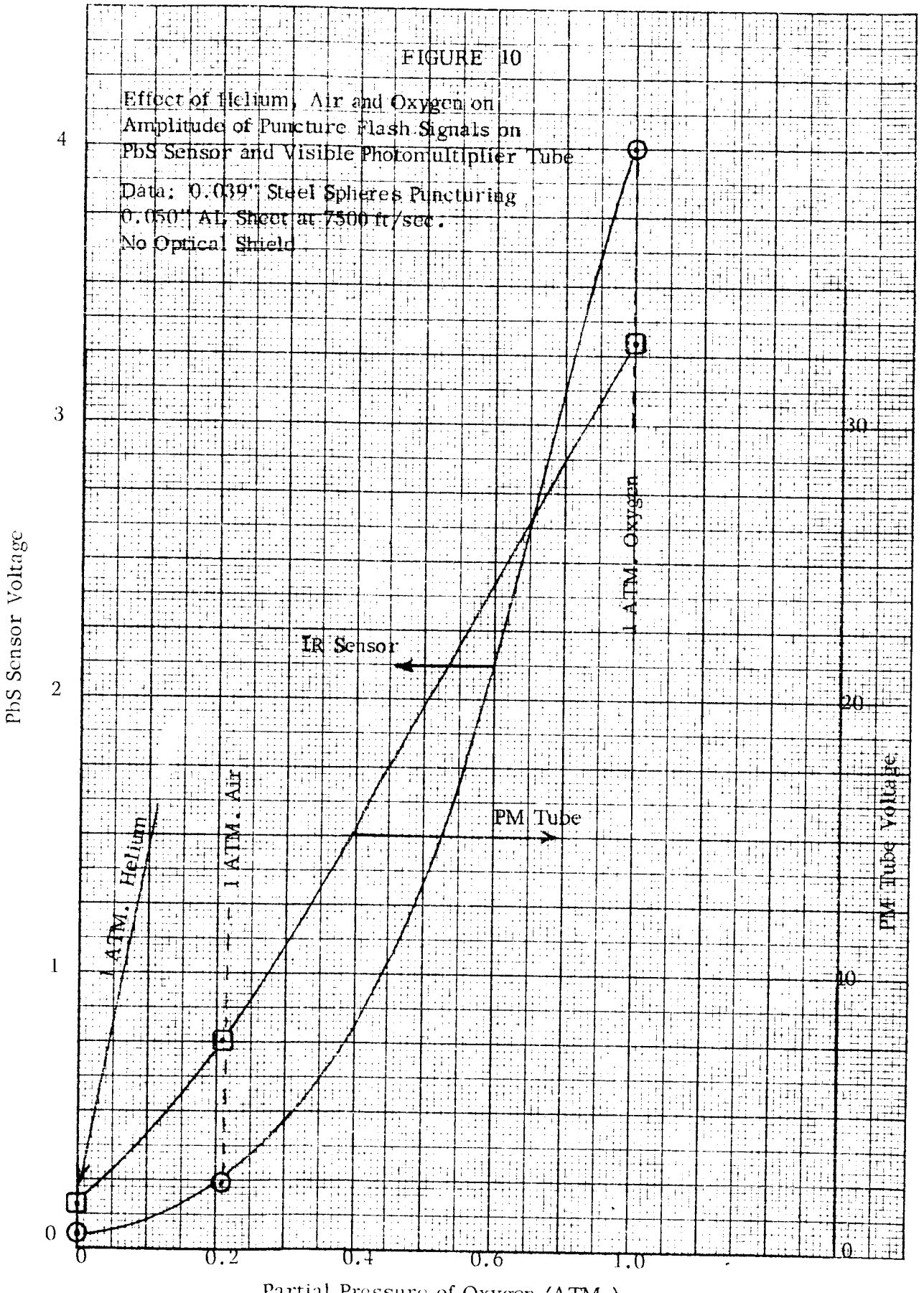

FIGURE 11

Time Variation of PM Tube Signals for Punctures into Oxygen and Helium, Showing Ejecta Cone Radiation Prior to Main Back-Spatter Flash.

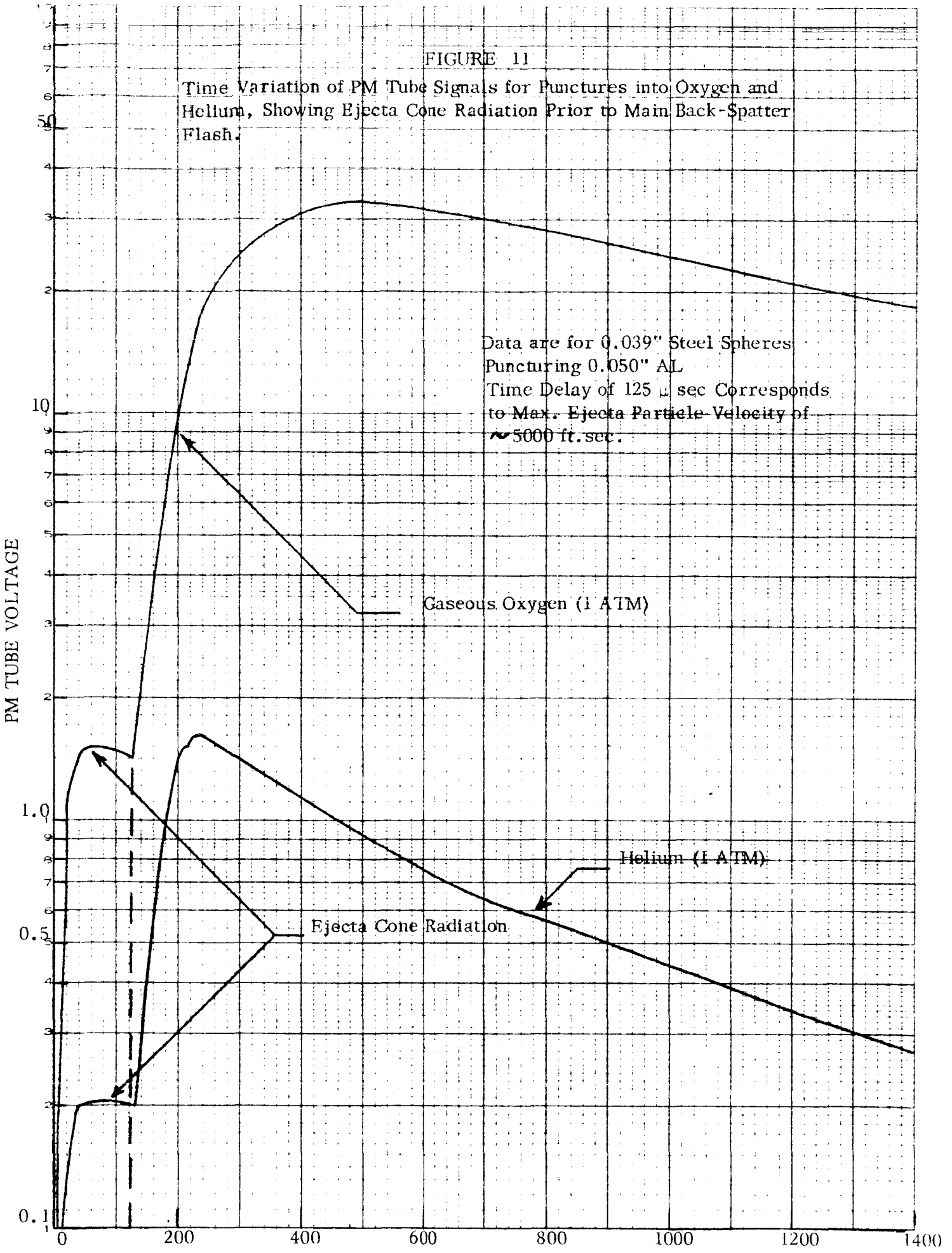

FREDERICK POST COMPANY 3117G370 SEM. LOGARITHMIC 3 3-1/3" CYCLES

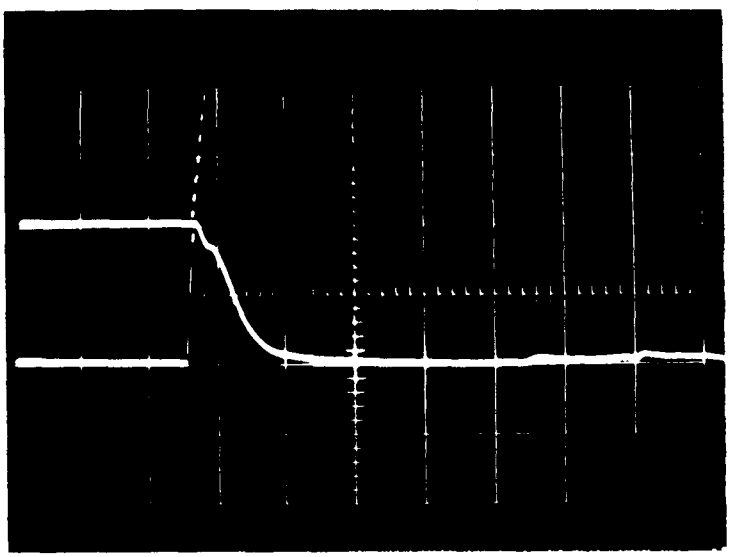

Figure 12

Oscillogram of Puncture Flash, Sidewinder Sensor and Photomultiplier Tube, (RCA 6199).

.025" steel ball through .050" Al. LOX level above target and below sensor, 7500 ft/sec, no optical shield.

PbS - Upper Trace: Vertical Gain - 0.5 v/cm

PM - Lower Trace: Vertical Gain - 10 v/cm

Sweep - 0.5 ms/cm

was deformed severely from the pressure pulse produced in the liquid immediately behind the puncture point.

For shot 5/16C, the PM tube was disconnected and a second PbS sensor was used which was immersed in liquid oxygen. The liquid level was about one inch below the puncture point so the ejecta entered into gaseous 0_2. The oscillogram showed a very slight signal ($\sim$ 0.1 volt) from the upper sensor which was in gaseous oxygen and no discernable signal from the PbS sensor immersed in liquid. It is possible that fog from air moisture may have blinded the upper sensor and bubbles from boiling of liquid oxygen may have prevented the lower sensor from detecting the flash. A contributing factor in each case was the large increase in sensor resistance as the sensors cooled down, which decreased the sensitivity because the series bias resistor was not increased correspondingly.

4. Analysis of Data Taken With a Five Inch Long Optical Shield

The data in Group II of Table I were taken primarily to provide data on punctures through aluminum for comparison with punctures through stainless steel which were reported in Reference 2. Therefore the optical view conditions of the PbS sensors were made identical.

Figure 13 shows the PbS sensor signals plotted against the impact kinetic energy parameter ($M_p V_p^2$). The solid points were taken from Table I, while the open points are from Reference 2. It is seen that the data for steel spheres through 0.050" aluminum in hard vacuum show a trend very much like those for steel spheres through 0.0204" stainless steel in hard vacuum, but with an amplitude about 4 to 5 times lower. For punctures through aluminum, the points for both Pyrex and sapphire spheres seem to fall a factor of two below the curve for steel spheres. It may be noted that the point for a 1/32 inch sapphire sphere through 0.0204" stainless steel from Reference 2 also appeared to be a factor of two lower than for steel spheres. It seems probable that this anomalous behavior of the puncture flash for sapphire and Pyrex, which are transparent oxides, may be related to Gehring and Charter's anomalously low impact flash obtained with Pyrex as compared to metals (Ref. 6). One might tentatively conclude that the plasma produced by oxides does not emit infrared radiation as strongly as for the metals.

Figure 13

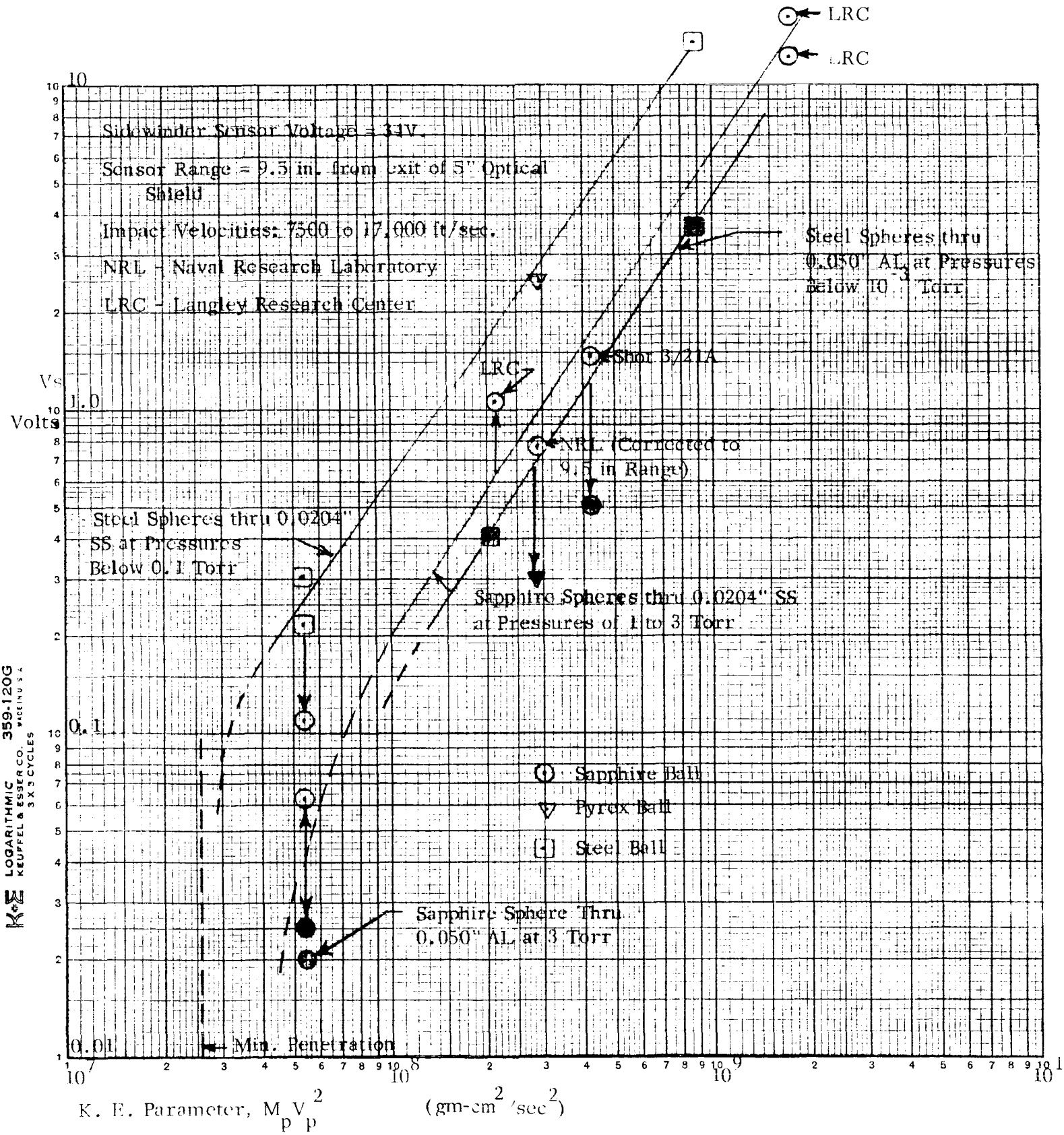

PbS Sensor Signal vs. Ball Kinetic Energy Parameter for Punctures Through 0.0204" Stainless Steel and 0.050" Aluminum Sheets at Various Air Pressure Levels.

Figure 13 also shows an additional point on the curve for punctures by sapphire spheres through 0.0204" stainless steel at air pressures of 1 to 3 Torr which is a repetition of a shot from Reference 2, showing there is considerable variability in signals obtained at kinetic energies only slightly greater than required for puncture.

Figure 14 shows the photomultiplier tube data as a function of kinetic energy of the impact for punctures at 7500 ft/sec through 0.050 inch aluminum at pressures between 4×10^{-4} and 6×10^{-4} Torr. It is seen that the data for steel spheres shows a variation of the visible signal with the square of the kinetic energy as compared with a variation of the PbS infrared signal (from Figure 13) with the 1.65 power of the kinetic energy.

It is also noted that the visible signal for a Pyrex sphere falls more than a factor of 10 lower than the curve for steel spheres, whereas the sapphire sphere appears to give a larger visible signal than the data for steel spheres.

By comparing the data from Figures 13 and 14, it appears that a sapphire sphere produces a puncture flash which is more intense in the visible, but less intense in the infrared, than a steel sphere of the same kinetic energy. A Pyrex sphere penetrating aluminum produces a puncture flash which is less intense in both the visible and infrared than a steel sphere of the same kinetic energy.

D. Determination of Equivalent Color Temperature of Puncture Flash Radiation

Theoretically the temperature of a grey body emitter may be determined by observing the radiation emitted at two discrete wavelengths. The temperature is a function of the ratio of the radiant intensities per unit wavelength at the two wavelengths, which may easily be derived from Planck's radiation law (Ref. 12).

For sensors having a finite spectral response, such as an RCA 6199 photomultiplier tube which responds from 0.32 to 0.54 microns, and a lead sulfide sensor which responds over the range out to 2.5 microns, the theoretical response is more complicated. However, it was expected that an empirical calibration of the ratio of the two signals against temperature of a known source might permit interpretation of puncture flash signal ratios in terms of equivalent grey body temperature of the source. Accordingly, the photomultiplier tube and PbS sensor which had been used to record

Figure 14

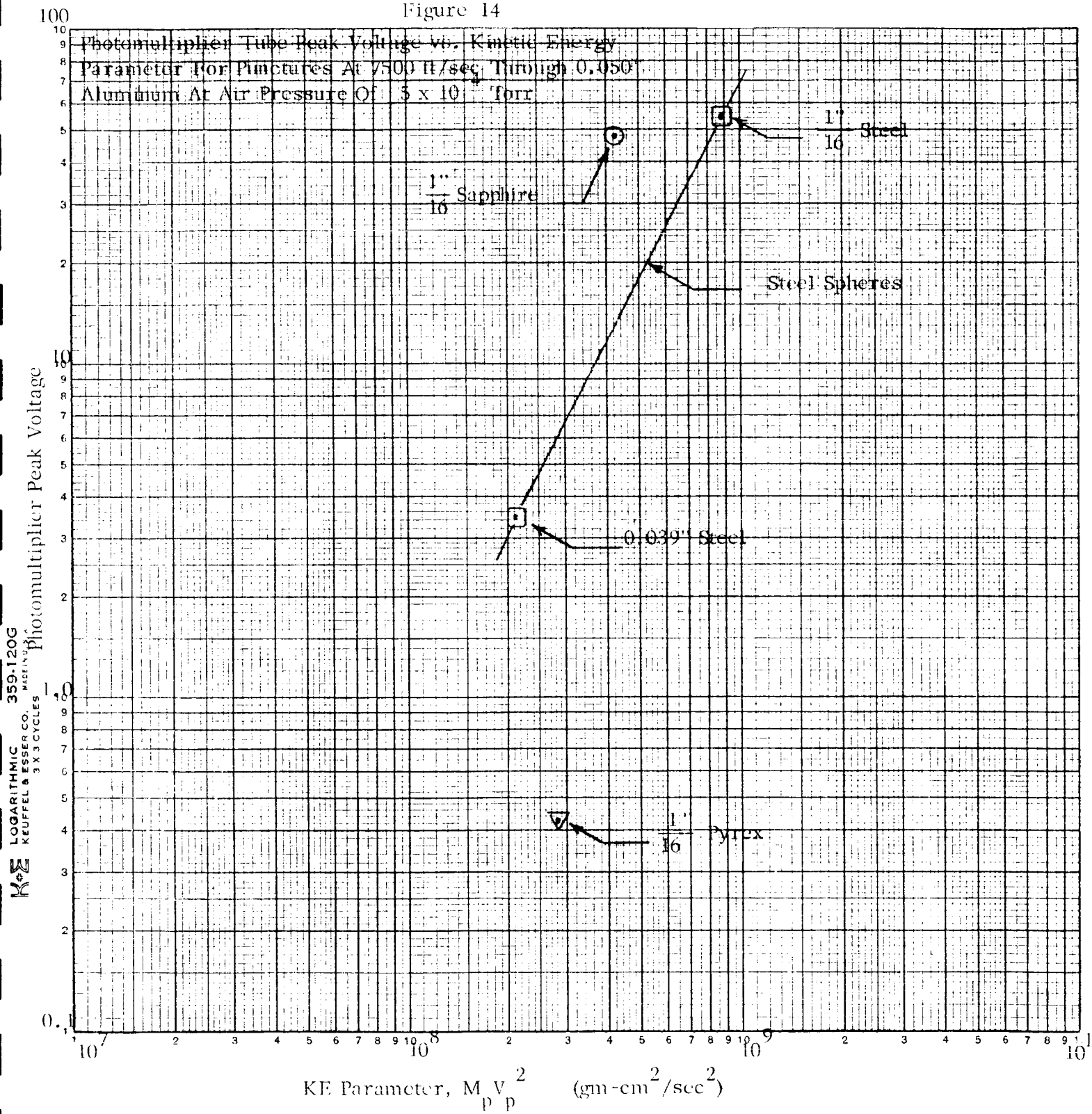
Photomultiplier Tube Peak Voltage vs. Kinetic Energy Parameter For Punctures At 7500 ft/sec Through 0.050" Aluminum At Air Pressure Of 5 x 10⁻⁴ Torr
1" / 16 Steel
1" / 16 Sapphire
Steel Spheres
0.039" Steel
1" / 16 Pyrex
Photomultiplier Peak Voltage
KE Parameter, M_p V_p^2 (gm-cm^2/sec^2)
LOGARITHMIC KEUFFEL & ESSER CO. 3 X 3 CYCLES 359-120G

puncture flash measurements were calibrated against a tungsten filament light source whose temperature was measured with a Model 95 Micro-Optical Pyrometer. The light beam was mechanically chopped at 6 pulses per second with a pulse duration of approximately 9 milliseconds. Figure 15 shows a typical oscillogram of the sensor waveforms obtained, from which the peak voltages of the PM tube and IR sensor were measured.

Figure 16 shows a plot of the two sensor outputs as a function of source temperature, as well as the ratio of the signals. It is seen that the ratio of the PM tube signal to the IR sensor signal is a steeply varying function of temperature only over the relatively narrow temperature range from 2700°F (1750°K) to 4000°F (2500°K). At somewhat higher temperatures, the ratio of signals is relatively constant and does not provide an accurate temperature measurement. This result is related to the relatively flat response of a PbS sensor and the high response of the PM tube to source temperatures in the range above 2500°K.

It is clear that a broader temperature range of applicability could be obtained by selecting sensors with more favorable response characteristics. In particular, the use of optical bandpass filters to limit the wavelengths of observation would be desired. The two wavelengths should also be chosen to remain on either the long-wavelength or short-wavelength side of the Planck distribution over the desired range of temperature measurement. For example, to cover the temperature range from 2000°K to 6000°K, both wavelengths should be greater than 1.4 microns or less than 0.5 microns.

The experimental measurements of the ratio of photomultiplier tube voltage to PbS sensor voltage are tabulated in Table II for all punctures into vacuum at pressures below 3 Torr. It is seen that the ratio is approximately 14 for steel spheres and 14 for Pyrex spheres but a much higher value near 80 for sapphire spheres.

It appears that both steel and Pyrex spheres give signal ratios which are not far different from the value of 10 obtained in the calibration tests for a tungsten source temperature of 2500°K to 3000°K.

However, the sapphire (Al_2O_3) spheres appear to emit strongly in the visible relative to the infrared. One may postulate that this effect may be partially due to strong emission of the aluminum doublet lines near 3950 Angstroms by the plasma

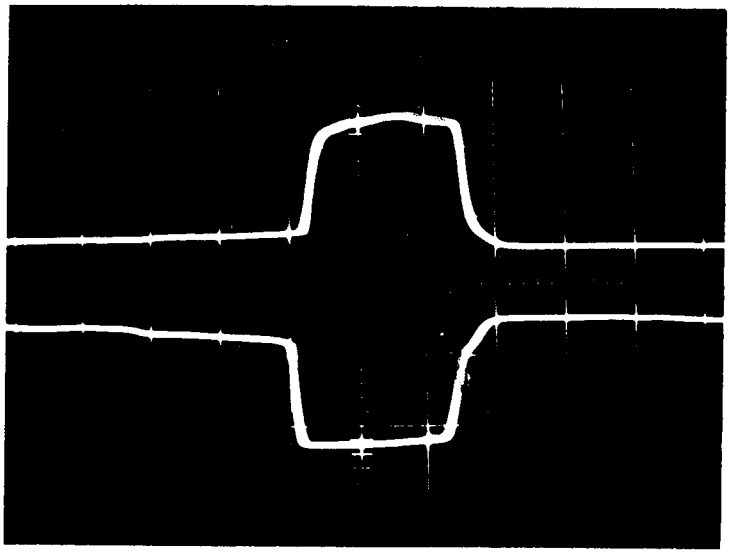

Figure 15

Oscillogram of Calibration Pulse, Sidewinder Sensor and Photomultiplier RCA-6199).

4180^{o}F Tungsten Filament Light Chopped 6 Pulses/Sec.

PbS - Upper Trace: Vertical Gain - 1 v/cm

PM - Lower Trace: Vertical Gain - 10 v/cm

Sweep - 4 ms/cm

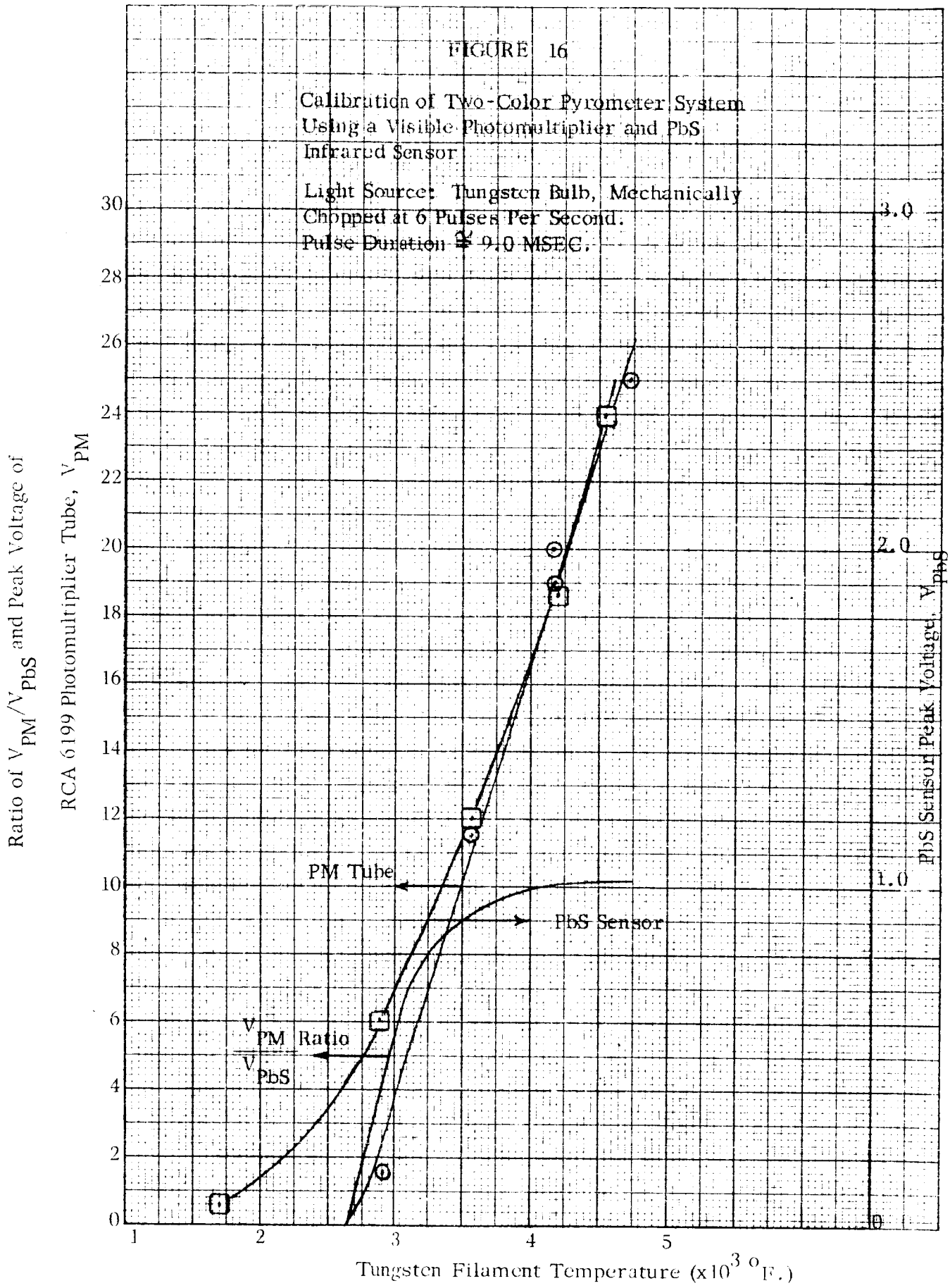

TABLE II

Ratio of Visible to Infrared Signal for various sphere materials at air pressures below 3 Torr.

Material	Diameter	Shot No.	Ratio: $\frac{V_{PM}}{V_{PbS}}$
Steel	0.039"	6/5D	9
Steel	0.039"	5/23B	18.4
Steel	1/16"	5/27L	15.
		Average Ratio:	14
Pyrex	1/16"	6/3F	14
Sapphire	1/16"	5/29I	96
Sapphire	1/32"	6/4H	71
Sapphire	1/32"	6/5H	>65
		Average Ratio:	80

produced when Al_2O_3 and Al ejecta particles impinge on the aluminum back spatter plate. These spectral lines are within the response range of the RCA 6199 photomultiplier tube. Also these lines have been observed spectrographically by Bull (Ref. 7) in the case of aluminum impacts on aluminum, and by Gehring (Ref. 6) in the case of nylon impacts on aluminum. However, it seems more likely that the high signal ratio for impacts of sapphire may be associated with a suppressed emission in the infrared as compared to steel and Pyrex.

Inspection of Figure 8 which shows the sensor signals obtained at the Naval Research Laboratory (for the puncture of a 1/32 inch sapphire sphere through 0.0204 inch type 301 stainless steel at 17,000 ft/sec) shows that the ratio of the visible PM tube signal to the PbS sensor signal is approximately 17, which is much lower than the ratio of more than 65 observed for a similar sphere at 7500 ft/sec in the Exotech facility. It is believed that this difference may be caused by the soft fiber-board witness plate at NRL as compared to an aluminum back-spatter plate at Exotech.

V. DEVELOPMENT OF LABORATORY CALIBRATION MODEL OF A METEOROID PUNCTURE DETECTION SYSTEM

A. Objective

The objective of the development program has been to provide a puncture detection system which can be calibrated in a variety of laboratory hypervelocity facilities to determine the infrared signal output produced by puncture flash as a function of target damage, such as hole size and to permit correlation of these parameters with the dynamic properties of the projectile, such as momentum and kinetic energy.

The system which has been developed consists of three major components:

1. A PbS infrared sensor
2. A logarithmic amplifier
3. A pulse voltage readout unit.

The amplifier and PbS sensor are powered by dry cell batteries, and the readout unit operates on 110 volt 60 cycle AC power. The system is portable and will permit visual readout of the infrared signal amplitude within 10 seconds after exposure of the sensor to a puncture flash (or impact flash) in laboratory hypervelocity facilities.

B. Methods for Making Puncture Flash Measurements

The properties of a puncture flash (or impact flash) of radiation produced by hypervelocity impact which can be readily measured are:

1. The peak intensity of the signal from a particular visible or infrared sensor.
2. The waveform (time variation) of the signal from a particular sensor.
3. The spectral distribution of the time-integrated signal as obtained with a spectrograph.
4. The time-resolved spectral distribution as obtained with a spectrograph and streak camera.
5. The time-resolved spectral distribution in selected bandwidths as obtained from fast response sensors using bandpass filters.

Of these techniques, the most simple is the measurement of peak intensity with a particular sensor. It has been shown that the peak intensity of sensor signals can be correlated with projectile and target parameters. Therefore the laboratory calibration model is designed to measure peak intensity of the signal using a calibrated amplifier and readout unit. An oscilloscope with camera can also be used as the amplifier readout unit in case it is desired to record the shape of the sensor signal pulse.

C. Selection of Optical Sensor

The optical sensors most suitable for detecting the visible and infrared radiation produced by puncture flash include photomultiplier tubes and photovoltaic sensors, which respond mainly in the visible, and photoconductive infrared sensors, which respond throughout the visible as well as in the infrared.

Experiments have shown (Ref. 2) that under conditions of a barely penetrating impact, practically no visible radiation may be produced, whereas the puncture flash is readily detectable by a PbS photoconductive infrared sensor at a range of 36 feet. This fact, coupled with the simple, rugged, reliable, environment-insensitive, and inexpensive features of the PbS sensor have led to its selection as the most suitable sensor for the laboratory model and potentially for a flight model of the puncture detection system.

The PbS sensor used is a standard production unit of the type supplied by Infrared Industries Incorporated for the Sidewinder missile. It has a dark resistance of approximately 680,000 ohms at 20° C.

The sensor is used in series with a 680,000 ohm load resistor in the amplifier input circuit shown in Figure 17. A battery is used to apply a voltage of 67.5 volts, of which one-half appears across the sensor.

Upon exposure to a pulse of radiation, the sensor resistance decreases by an amount ΔR, producing a voltage change across the load resistor given by:

$$\Delta V_{RL} = \frac{V_B R_L \Delta R}{(R+R_L)^2}$$

BLOCK DIAGRAM OF SYSTEM

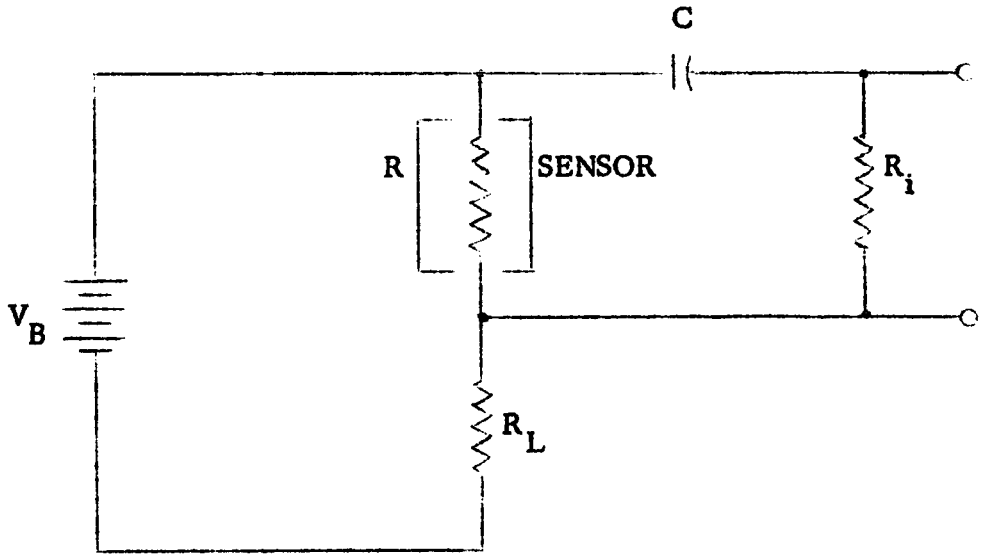

SENSOR SYSTEM BLOCK DIAGRAM AND INPUT CIRCUIT

Figure 17

The maximum signal is obtained when $R = R_L$, in which case

$$\Delta V_{RL} = \frac{V_B \Delta R}{4R}$$

This voltage pulse is passed by capacitor C to the input of a preamplifier.

The design of the mounting for the PbS sensor depends on the application requirements. However, the sensor mounting shown in the drawing of Figure 18 and the photograph in Figure 19 is suitable for mounting in the vacuum facilities of a typical hypervelocity facility. It incorporates a glass-to-metal electrical feed-through and O-Ring seals.

D. Electronic Amplifier

Experiments have shown that the puncture flash signals produced by a PbS sensor may vary in amplitude from about 15 volts at a sensor range of 9.5 inches to as low as about 50 microvolts at a sensor range of 36 feet. Since it is not possible a priori to predict the size of the signal expected from a given shot with good accuracy, it is desirable to have an amplifier with a logarithmic gain characteristic, so that the readout unit or oscilloscope gives a readable signal without going off scale.

Experiments were conducted with a Barnes Engineering Model LA-3A logarithmic amplifier to determine its suitability for this application. However it was found that the preamplifier section of the LA-3A was unstable and would produce self-oscillations and motor-boating when used with input impedance values in the range corresponding to the desired sensor resistance. Therefore a more stable preamplifier (designated PA-1A) was fabricated and used to feed into the logarithmic section of the Barnes LA-3A amplifier.

The circuit of the PA-1A preamplifier is shown in Figure 20 and a summary of its operating characteristics is shown in Table III.

The first stage of the preamplifier is an advanced double diffused planar silicon transistor (No. 2N2586) of grounded emitter configuration operating in the small signal mode at a collector current of 2.64 μ amps. Operating under the conditions of $V_{CE} = 5.0$ volts, I_C of 1 μ amp, R_g of one megohm, the manufacturer

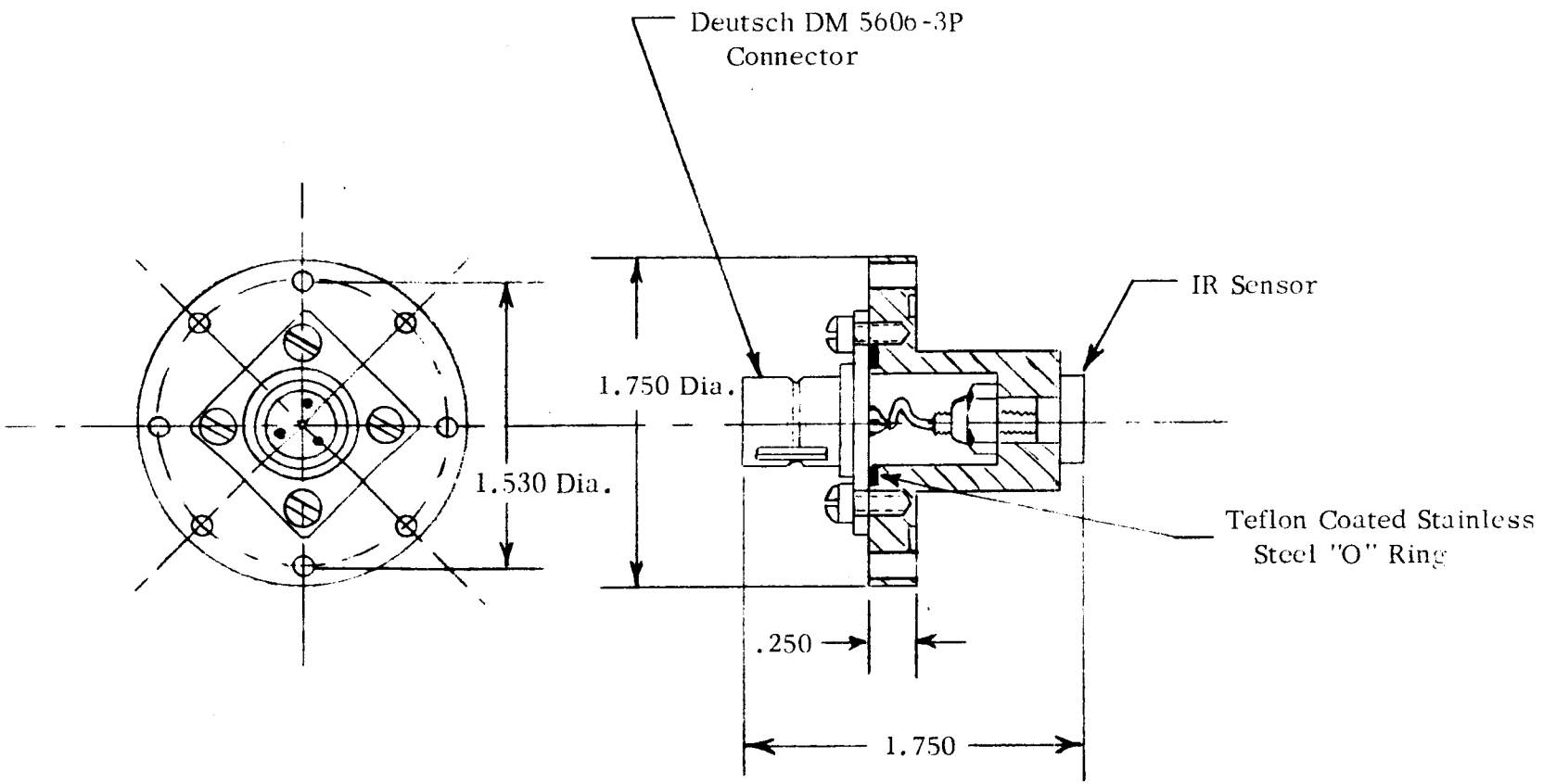

SENSOR ASSEMBLY

FIGURE 18

Figure 19

Photograph Of Sensor Mounting

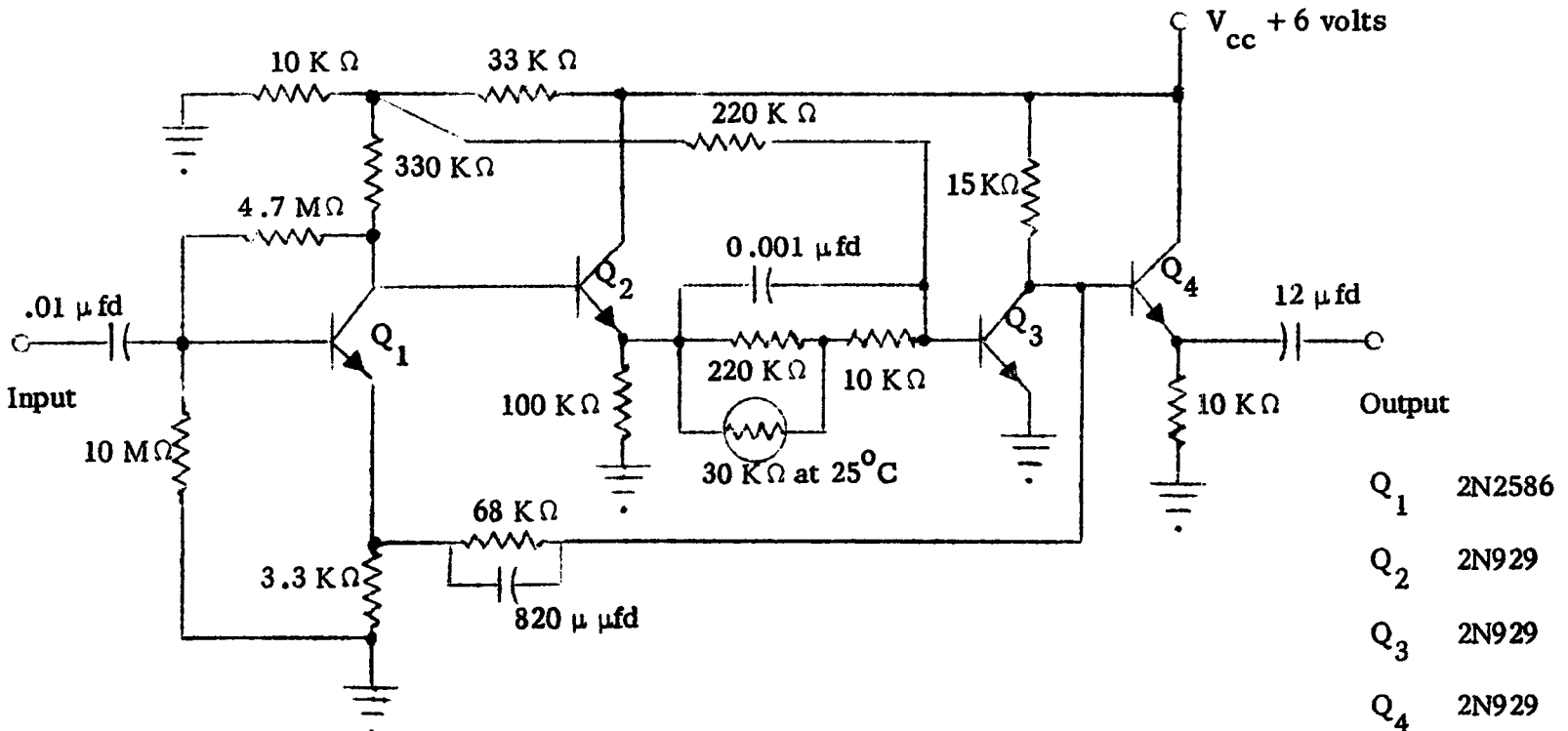

Exotech PA-1A Preamplifier Circuit

FIGURE 20

TABLE III

Characteristics Of Exotech PA-1A Preamplifier And Barnes LA-3A Operational Amplifier

PA-1A Preamplifier

Input Impedance	> 2 megohms
Output Impedance	1200 ohms
Frequency Response	100 cps - 1800 cps (3db down)
Voltage Gain	16
Maximum Output	4 volts
Noise Figure	3 db (R_s = 680K ohms)
Power Required @ 22 volts	3×10^{-3} watt

Barnes LA-3A Operational Amplifier (Logarithmic)

Output Impedance	< 150 ohms (Load should be > 2000 ohms)
Frequency Response	300 - 1200 cps (for low level signals)
Voltage Gain	2500 (for low level signals)
Maximum Output	6 volts
Noise Voltage	30 mv RMS (R_s = 100K ohms)
Log Transfer Slope	1 volt/20 db
Power Required @ 22 volts	5.3×10^{-2} watt

guaranteed a minimum h_{fe} of 80 and a maximum spot noise figure of 3.5 db at 1 KC. The stages immediately following the first stage are conventional 2N929 transistors. The preamplifier gain is 16 with an input impedance greater than 2 megohm; the output impedance is less than 1.5 K ohm and the equivalent input noise is approximately 5 μ volts RMS.

The broadband preamplifier noise figure measurement is shown in Figure 21. It is seen that the measured noise figure falls on the manufacturer's curve for the first stage 2N2586 transistor.

The circuit of the operational amplifier section of the Barnes LA-3A amplifier, as shown in Figure 22, incorporates four stages of amplification with a multiple feedback loop system. The amplitude of the signal controls the number of diode feedback loops, which in turn control the system gain. The output signal is approximately proportional to the logarithm of the input signal over a range of four decades of the input signal (from 100 microvolts to 1 volt). The characteristics of the logarithmic amplifier are shown in Table III.

E. Pulse Voltage Readout Unit

The amplitude of an output pulse from the amplifier, or directly from an infrared sensor, is measured by means of a pulse voltage readout unit. This unit incorporates a capacitor storage network and an electrometer amplifier which operates a DC voltmeter for visual readout. The circuit is shown in Figure 23 and its simplified circuit equivalent is shown in Figure 24.

When a positive unidirectional voltage pulse is applied at the input, its maximum value is stored on the filter capacitors C_2 and C_3 which hold the grid of the cathode follower tube Q_1 at the peak voltage for a sufficient period of time to be read out before leaking off. The readout is accomplished by a stable differential amplifier composed of electron tubes Q_2 and Q_3, which operates a Triplett Mod. 420-u voltmeter.

A damping circuit (R_3 and C_4) is included at the input of the differential amplifier to eliminate any voltage surges which could damage the voltmeter movement.

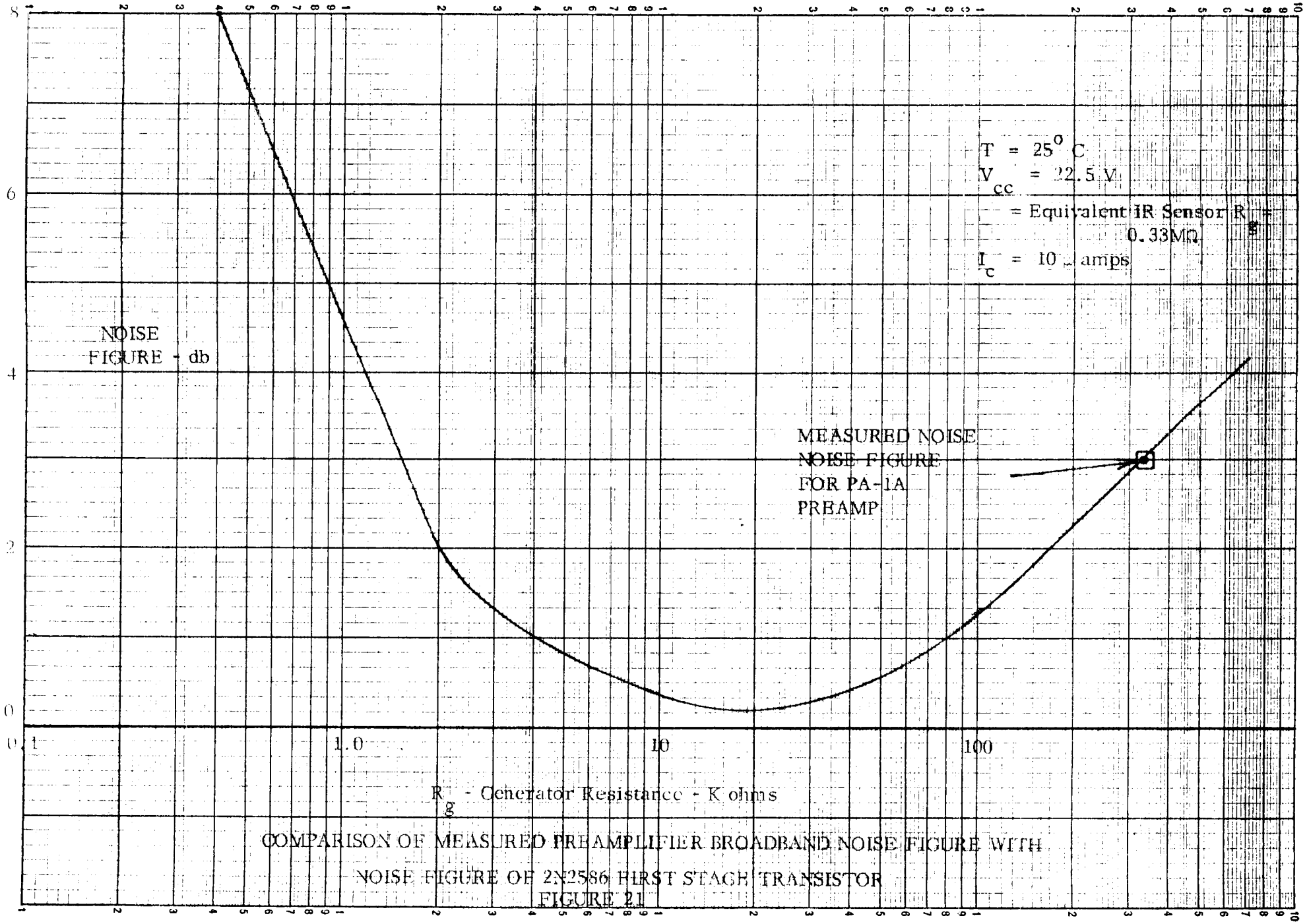

COMPARISON OF MEASURED PREAMPLIFIER BROADBAND NOISE FIGURE WITH NOISE FIGURE OF 2N2586 FIRST STAGE TRANSISTOR

FIGURE 21

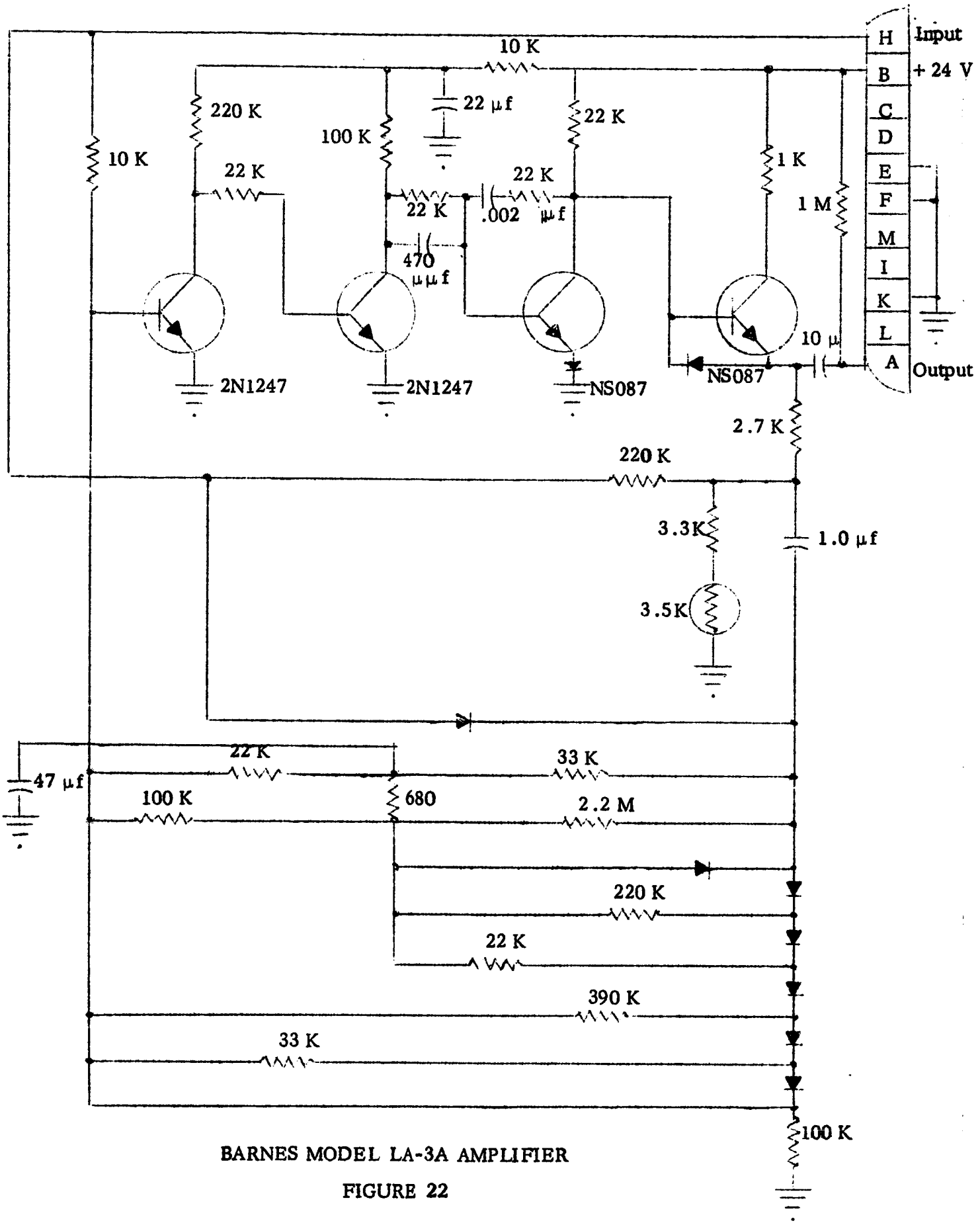

BARNES MODEL LA-3A AMPLIFIER

FIGURE 22

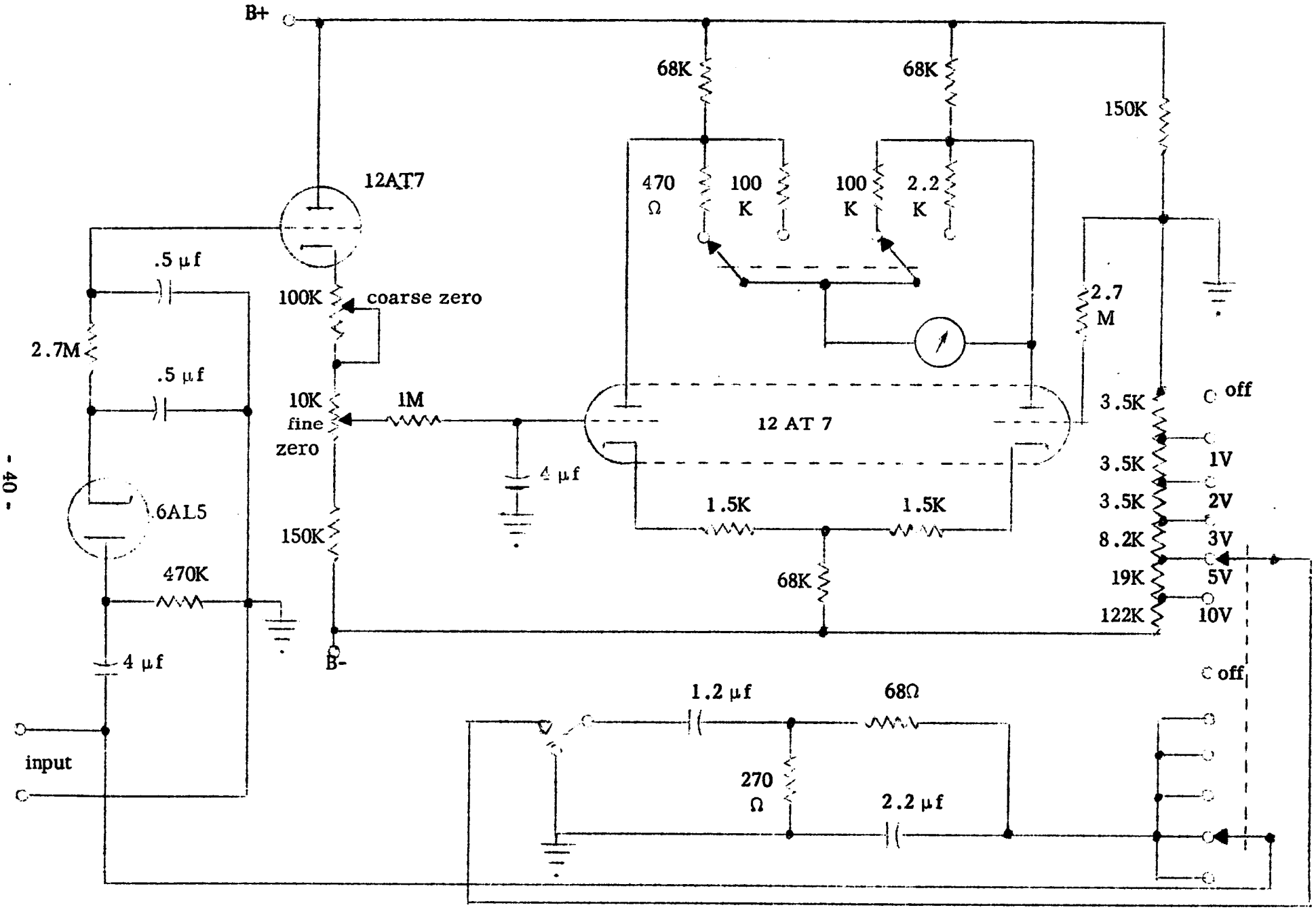

Figure 23 SCHEMATIC CIRCUIT DIAGRAM OF PULSE VOLTAGE READOUT UNIT

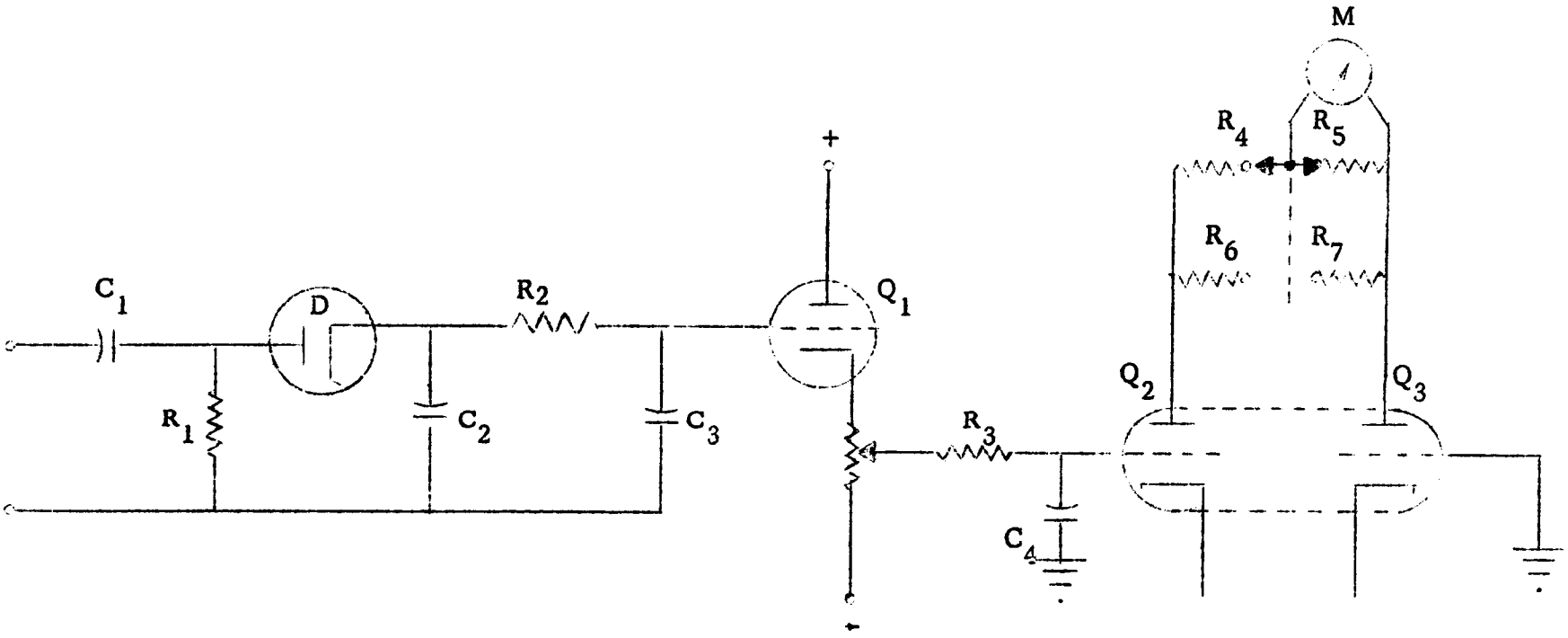

FIGURE 24 OPERATIONAL DIAGRAM OF THE ELECTROMETER READOUT UNIT

A selector switch controls the range of the meter to be either 3 volts or 10 volts, full scale.

F. Operational Characteristics of the Puncture Detection System

The laboratory calibration model will measure sensor pulses having a 300 μ second rise time over the dynamic range from 100 x 10^{-6} to 10.0 volts. The pulse voltage readout unit, by itself, will accept pulses from 400 mv to 3 volts on the 3 volt scale and 500 mv to 10 volts on the 10 volt scale, which are selectable on the front panel. The additional range down to 100 x 10^{-6} volts is attained by switching in the preamplifier-amplifier unit. The measured transfer function for the preamplifier-amplifier unit is shown in Figure 25, which shows the voltage available to the input of the readout unit as a function of preamplifier input signal. The transfer characteristics for both the 3 volt and 10 volt ranges of the readout unit are shown in Figure 26. The calibration in Figure 26 is to be utilized for all readings when the anticipated voltage peak is greater than 0.4 volts, in which case, the preamplifier-amplifier unit can be by-passed. The readout unit was calibrated with 150 μ second, 220 μ second, and 330 μ second pulse rise times and it is shown in Figure 26 that the output is substantially independent of pulse rise time in this range, which is typical of puncture flash signals. The calibration data for these points are tabulated in Table IV. For sensor signals below 0.4 volt, the preamplifier-amplifier unit should be switched into the circuit, and the calibration for the complete system is shown in Figure 27.

Sensor bias voltage at 67-1/2 volts is applied from an internal battery in the amplifer case and is available at the sensor connection. A 680 K ohm bias resistor is also in the circuit in the amplifier case and optimum operating conditions are met if the sensor dark resistance has the same value of resistance as the bias resistor.

An internal calibration network has been incorporated that will produce a pulse of uniform shape with an adjustable height. The pulse calibration circuit is composed of a capacitance and resistance network which gives a uniform pulse when the capacitor is shorted to ground by a manual switch. The pulse time constant is fixed at 150 μ seconds rise time by the RC time constant of the circuit (68 ohms and 2.2 μfd). The shape of the calibration pulse is shown in Figure 28. The calibration network is

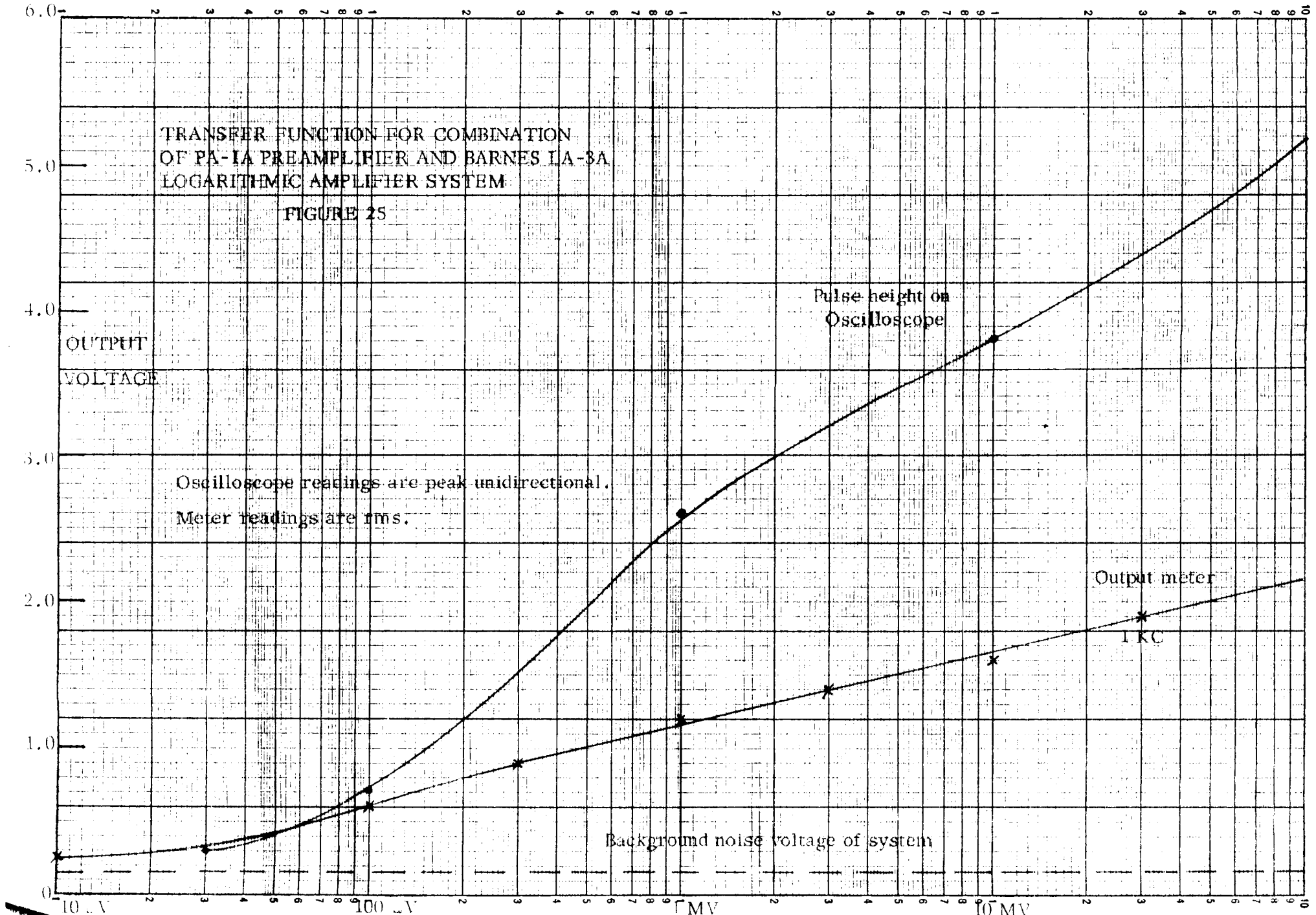

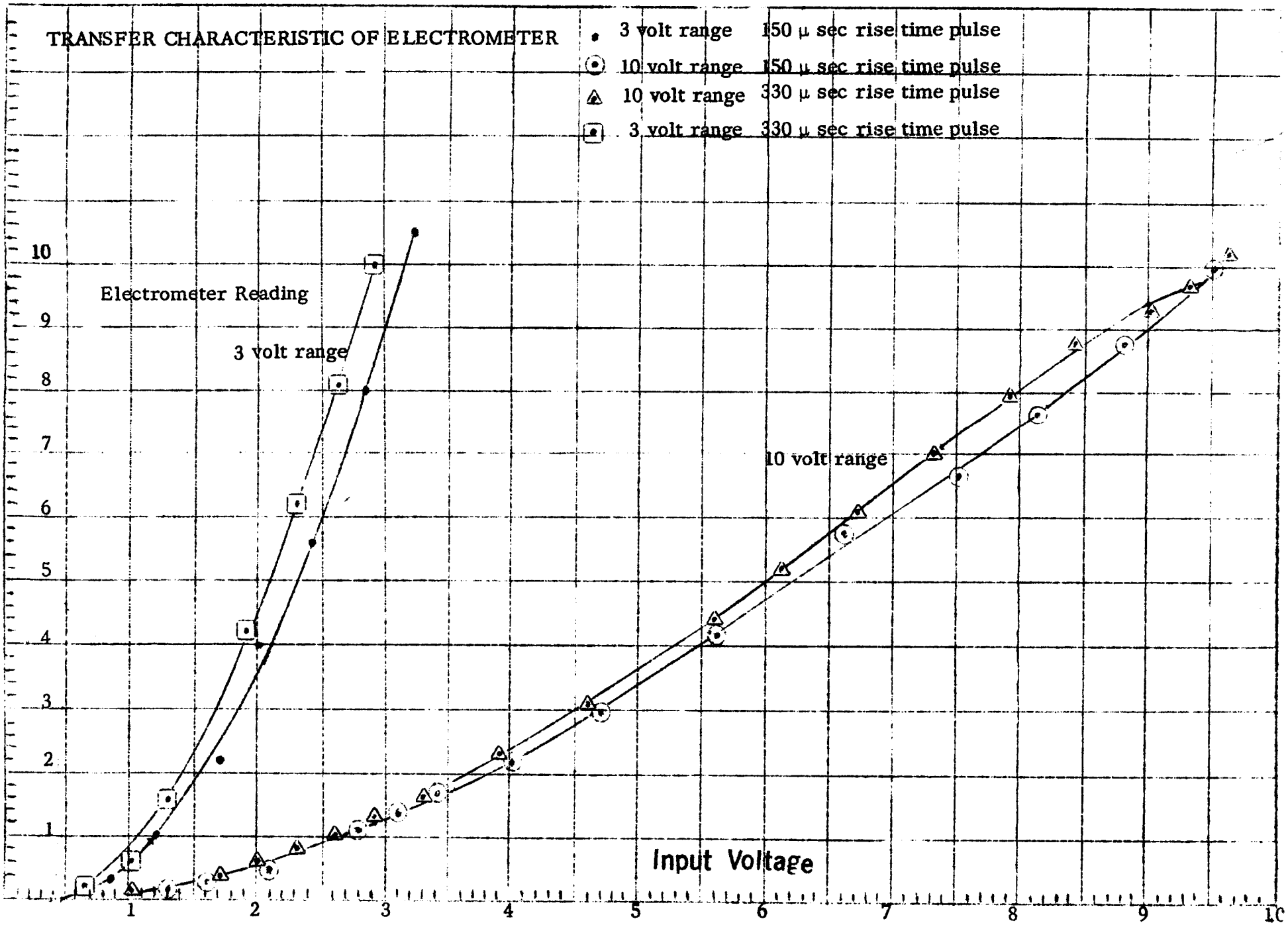

Figure 26 VOLTAGE PEAK OF UNIDIRECTIONAL PULSE INTO ELECTROMETER

TABLE IV

Table Of Calibration For Readout Unit

Applied Voltage	150 μ sec* Peak of Voltage Pulse	150 μ sec* Meter Reading	200 μ sec* Peak of Volt Pulse	200 μ sec* Meter	330 μ sec* Peak of V Pulse	330 μ sec* Meter
3 Volt Range						
1.5	0.43	0	0.4	<0.1	0.36	<0.1
3.0	0.84	0.3	0.8	0.3	0.64	0.2
4.5	1.2	1.0	1.2	0.8	1.0	0.6
6.0	1.7	2.2	1.5	2.0	1.3	1.6
7.5	2.0	4.0	1.9	3.4	1.6	1.9
9.0	2.4	5.6	2.2	5.1	1.9	4.2
10.5	2.8	8.0	2.6	7.1	2.3	6.2
12.0	3.2	10.5	3.0	9.4	2.6	8.1
13.5	-	-	-	-	2.9	10.0
10 Volt Range						
4.5	1.3	0.1	1.2	0.1	1.0	0.1
6.0	1.6	0.3	1.5	0.2	1.3	0.2
7.5	2.1	0.5	1.9	0.4	1.7	0.4
9.0	2.4	0.8	2.2	0.7	2.0	0.5
10.5	2.8	1.1	2.6	0.9	2.3	0.8
12.0	3.1	1.4	3.0	1.2	2.6	1.0
13.5	3.4	1.7	3.3	1.6	2.9	1.3
15.0	4.0	2.2	3.7	1.9	3.3	1.6
18.0	4.7	3.0	4.4	2.7	3.9	2.3
22.5	5.6	4.2	5.2	3.6	4.6	3.1

* Pulse Rise Time To 7[illegible]% Maximum:

TABLE IV CONTINUED

Applied Voltage	150 μ sec*		200 μ sec*		330 μ sec*	
	Peak of Voltage Pulse	Meter Reading	Peak of Volt Pulse	Meter	Peak of V Pulse	Meter
27	6.6	5.8	6.2	5.0	5.6	4.4
30	7.5	6.7	6.8	6.0	6.1	5.2
33	8.1	7.7	7.6	6.9	6.7	6.1
36	8.8	8.8	8.4	7.9	7.3	7.0
39	9.5	10.0	9.0	8.9	7.9	8.0
42	-	-	9.8	10.0	8.4	8.8
45	-	-	10.3	10.5	9.0	9.3
46.5	-	-	-	-	9.3	9.7
48	-	-	-	-	9.6	10.2

The battery voltage was utilized to produce a pulse through the calibration network. The tabulated peak of voltage value was read at the output of the calibration network with a Tektronix 531 A oscilloscope utilizing a type CA plug-in preamplifier.

* Pulse Rise Time To 75% Maximum.

Figure 27 CALIBRATION CURVES FOR LABORATORY CALIBRATION MODEL OF METEOROID PUNCTURE DETECTION SYSTEM, INCLUDING AMPLIFIER AND READOUT UNIT

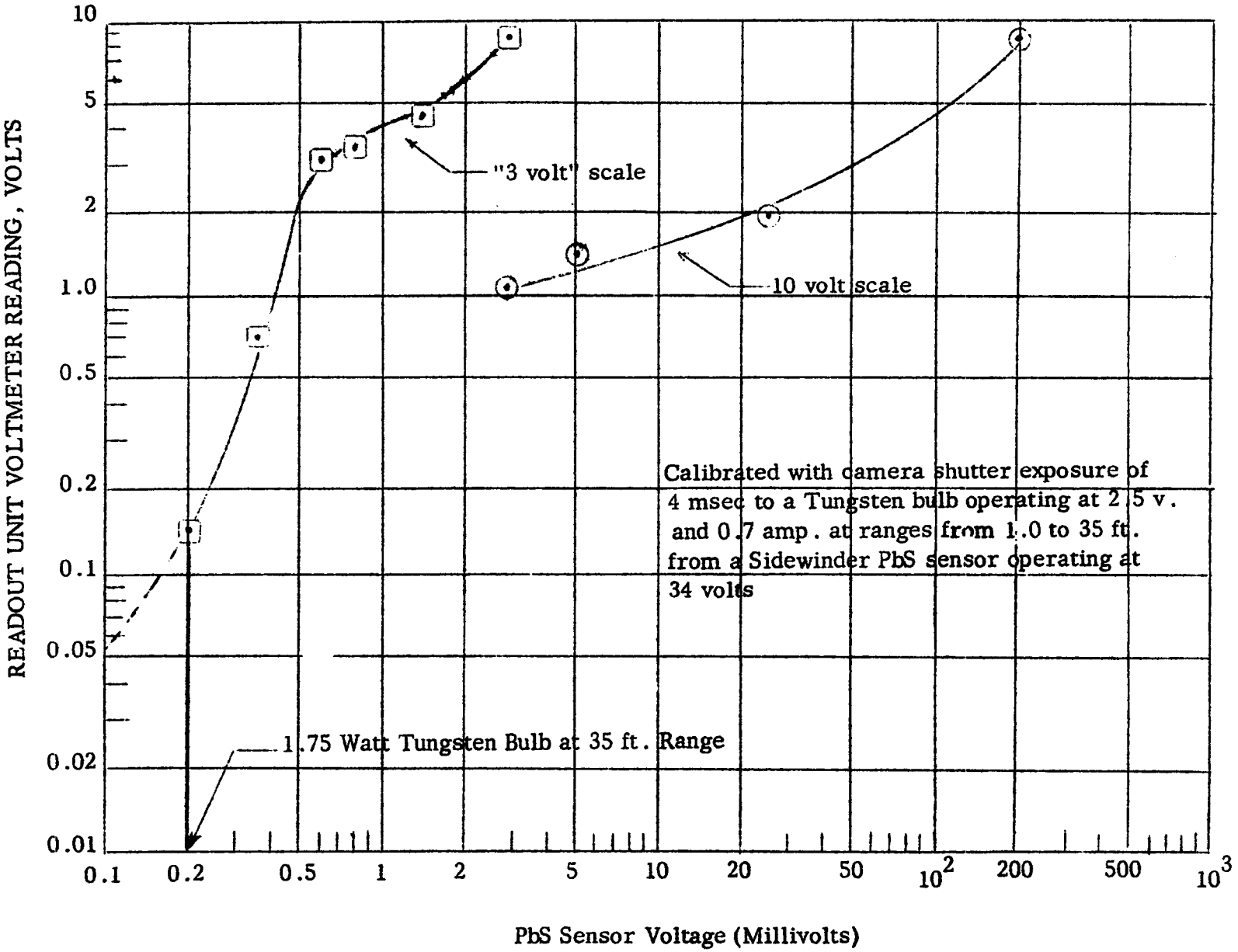

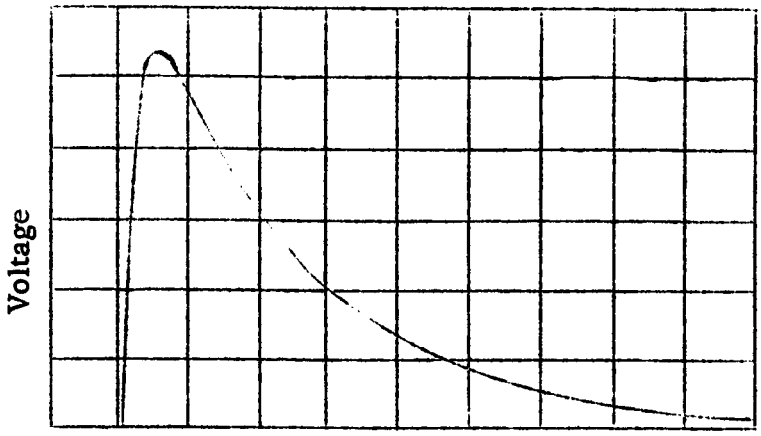

Figure 28 CALIBRATION PULSE FROM INTERNAL CALIBRATION NETWORK

in the readout instrument and is operated by selecting the pulse height desired with the calibrate selector switch, zeroing the meter with the zero adjustment, depressing the calibrate push button, holding in this position for five seconds, then releasing and observing the meter reading.

When using the instrument to record puncture flash measurements, the system should be calibrated as discussed above and then at least a one minute delay allowed for the meter to return to zero before firing the hypervelocity shot. The readout unit may be remotely located with a cable length of up to 50 feet for safety. The meter will normally reach maximum reading within ten seconds after the shot, and the movement is slow enough for easy visual reading of the maximum voltage.

The readout unit incorporates a line filter to prevent stray electrical noise from actuating the readout unit.

A photograph of the laboratory calibration model of the meteoroid puncture detection system, including sensor, amplifier, and readout units, is shown in Figure 29.

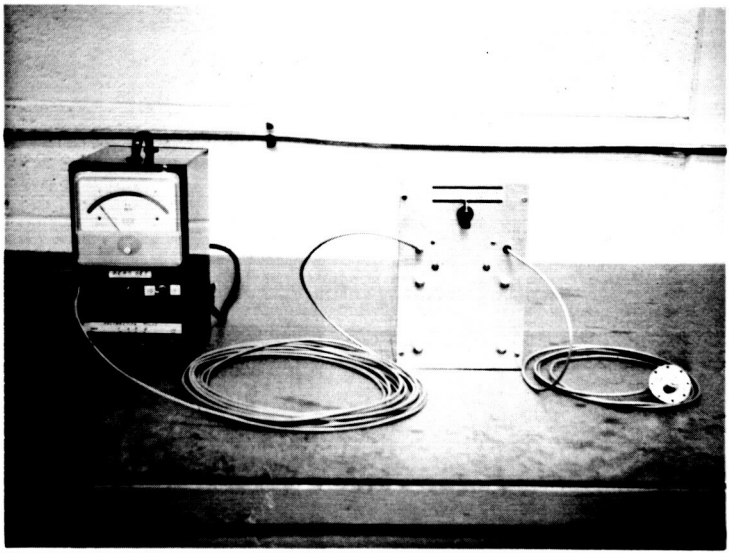

Figure 29

Laboratory Calibration Model Of The
Meteoroid Puncture Detection System

VI CONCLUSIONS

1. A laboratory calibration model of a meteoroid puncture detection system has been developed which permits measurement of the amplitude of infrared sensor signals produced by puncture flash over a range from approximately 100 microvolts to 8 volts.

2. Research on the puncture flash phenomena produced by puncture of small spheres at 7500 ft/sec through 50 mil Type 3003-H14 aluminum sheet in vacuum has verified that the infrared and visible sensor signals produced by steel spheres can be correlated with the kinetic energy of impact, as found for punctures through stainless steel.

3. As compared to steel spheres of the same kinetic energy, the puncture flash produced by Pyrex spheres appears anomalously low in both the visible and infrared signal, whereas the puncture flash produced by sapphire spheres appears to be low in the infrared but high in the visible.

4. The major contribution to the puncture flash signal is generally produced by the "back spatter flash" which is composed of multiple impact flashes as solid particles of ejecta strike the aluminum back spatter plate. The "ejecta cone radiation" emitted directly by the ejecta material itself is generally much lower in intensity than the back spatter flash.

5. The luminosity of the back spatter flash is increased, both in the infrared and the visible, by the presence of air and particularly oxygen in the target tank as compared to helium.

6. The puncture flash produced by a 0.039" steel sphere at 7500 ft/sec was greater in a vacuum of 5×10^{-4} Torr than in either helium or air at one atmosphere. However, the puncture flash in pure oxygen gas exceeded that in a vacuum, because chemical oxidation reactions become predominant over the aerodynamic effects (drag on ejecta

and inhibition of expansion of the plasma from the back spatter plate) which tend to reduce the puncture flash signals observed at the sensor locations in these experiments.

7. As compared to helium, the effect of a vacuum is somewhat more effective in increasing the luminosity of the puncture than the presence of oxygen when firing in air at one atmosphere pressure.

8. The ratios of visible photomultiplier tube signal to PbS sensor signal for punctures of stainless steel and Pyrex spheres through 50 mil aluminum were approximately the same as the ratio obtained when observing the chopped beam from a tungsten filament at a temperature of 2500°K to 3000°K. However, the ratios observed for punctures by sapphire spheres were much larger, indicating that the puncture flash is stronger in the visible and less intense in the infrared.

9. Additional research is needed to study the spectral distribution of the radiation emitted by puncture flash in order to determine how spectral measurements can be correlated with properties of the projectile to permit development of a meteoroid puncture gauge which would measure meteoroid properties such as velocity or material.

VII REFERENCES

1. Cooley, W. C. and Luckhardt, P. G., "Investigation of a Micrometeoroid Vehicle Damage Assessment System", Summary Report on Contract NAS 8-5033 with NASA-MSFC, Exotech Incorporated, Alexandria, Virginia, November 1962.

2. "Investigation of Feasibility of Infrared Detection of Meteoroid Punctures in Atlas Tanks", Summary Report on Contract NAS 9-1268 with NASA-MSC, Exotech Incorporated, Alexandria, Virginia, May 1963.

3. Atkins, W. W., "Flash Associated with High-Velocity Impact on Aluminum", Journal of Applied Physics, Vol. 26, No. 1, pp 126-7, January 1955.

4. Clark, W. H., Kadisch, R. R. and Grow, R. W., "Spectral Analysis of the Impact of Ultra-Velocity Copper Spheres into Copper Targets", Technical Report DSR-16, University of Utah, September 1, 1959.

5. Gehring, J. W. and Sieck, D. W., "A Study of the Phenomena of Impact Flash and its Relation to the Reaction of the Lunar Surface in the Impact of a Lunar Probe", ARS Lunar Missions Meeting, Cleveland, Ohio, ARS Paper 2476-62, July 1962.

6. Gehring, J. W. and Charters, A. C., "Meteoroid Impact on the Lunar Surface", Presented at the Sixth Hypervelocity Impact Symposium, Cleveland, Ohio, May 1, 1963.

7. Bull, G. V., McGill University, Montreal, Canada, Private Communication, May 1963.

8. MacCormack, R. W., "Investigation of Impact Flash at Low Ambient Pressures", Presented at the Sixth Hypervelocity Impact Symposium, Cleveland, Ohio, May 1, 1963.

9. Bull, G. V., "On the Impact of Pellets with Thin Plates, Theoretical Considerations-Part I", Arthur D. Little Report Number 63270-03-01, Prepared under Contract NAS 5-664, January 1962.

10. Friend, W. H., Miller, D. A., and Murphy, C. L., "The Hypervelocity Impact of Pellets with Thin Plates - Theoretical Considerations Part II", McGill University, Dept. of Mechanical Engineering, Report Rep. 62-8, October 1962.

11. Bjork, R. L., "Effects of Meteoroid Impact on Steel and Aluminum in Space, Rand Corp., p. 1662, December 16, 1958.

12. Vali, W. and De Voto, R. S., "A Two-Color Pyrometer for the Measurement of Temperature and Contamination Level in a Spark-Heated Hypervelocity Wind Tunnel", Technical Documentary Report No. AEDC-TDR-62-174, August 1962.